OBLIQUE STRUCTURES DEVELOPED IN HOMOGENEOUS ANISOTROPIC MATERIAL

OBLIQUE STRUCTURES DEVELOPED IN HOMOGENEOUS ANISOTROPIC MATERIAL

By

Peter I. Wallace

A Thesis Submitted
to the Faculty of Science
in Partial Fulfilment of the Requirements
for the Degree
Bachelor of Science

McMaster University

April 1973

Abstract

Layers of plasticene lubricated with talcum powder were compressed in directions perpendicular to the layering. Normal kink bands oblique to the principal compression direction were produced. These structures were predicted by Cosgrove (1972) after a theory developed by Biot (1965). Other multilayers, with the layering oblique to the principal compression direction, were compressed and these developed instabilities also.

The normal kink bands were analysed geometrically. It was found that variation in layer thickness provided the best description and also provided a statement of the state of strain of the final deformation.

Table of Contents

List of Figures and Tables

TABLES

FIGURES

31. Graph of area vs. number of layer for face of section 2, Experiment #5

32. Ductile Flow in the Multilayer during Kink Band Formation

Acknowledgements

I wish to thank Dr. P. Clifford for stimulating my interest in structural geology and Dr. J. Cosgrove for his expert guidence in the experimental work and for criticism of the draft of this thesis. I also wish to thank my wife for her understanding as I prepared the final copy.

1. Introduction

Kink bands are the names given to angular, steplike monoclines where the distance between adjacent parallel-plane axial surfaces does not exceed about 10 cm. (Dewey 1965, Ramsay 1967) The fold shape of different layers throughout the structure generally keeps constant, and the overall geometry form of kink bands is generally of the similar type but individual layers are of the parallel form (Figure 1)(Ramsay 1967). Kink bands and associated features are always found in material that has numerous parallel plane surfaces.

The development of kink bands has always been a problem. Buckling instabilities in certain multilayers were explained by relating the viscosity ratios of the layers (Biot 1961, Ramberg 1961a, 1961b, 1963, 1964). First a single layer was considered and then the same reasoning was applied to a multilayered sequence. This made the buckling behaviour fundamentally dependent upon the ratio of the properties of the adjacent layers. The theory failed to explain the features that resulted when the properties of the layers became alike. Biot (1965) developed a theory where he considered a homogeneous anisotropic material of the viscous, elastic, and visco-elastic types in order to predict the kinds of instabilities that would result if the material were stressed. The theory was especially useful because it accounted for all types of buckling instability.

Cosgrove (1972) developed Biot's theory to explain kink band formation. He found that if layers with a good anisotropy were compressed parallel to the layering conjugate reverse kink bands could form. These are the "classical" kink bands discussed in the literature. However, if compression took place normal to the layering conjugate normal kink bands could form. Here the terms normal and reverse kink bands are analogous to normal and reverse faults. (Figure 2)(Dewey 1965) In between these two layer orientations a variety of structures were predicted depending on the degree of anisotropy and the orientation of the original layering.

This thesis deals primarily with normal kink bands. Other authors have mentioned them (Cosgrove 1972, Cobbold et. al. 1971, Dewey 1965) but no complete description of their geometry was given. Experiments were performed to produce normal kink bands in layered material. These normal kink bands were subsequently analysed geometrically to provide an adequate description.

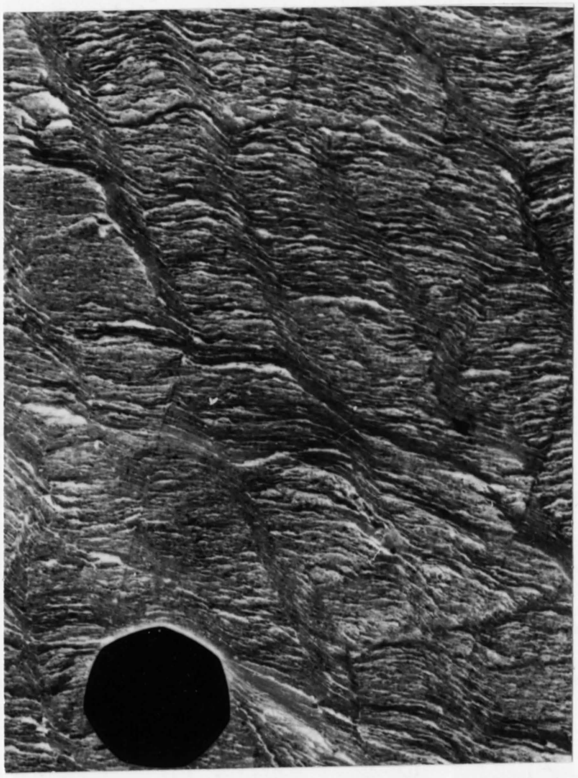

Figure 1

Normal kink bands in Devonian Slate, Tor Cross, S.E. Devon. (photo courtesy of Dr. J. Cosgrove)

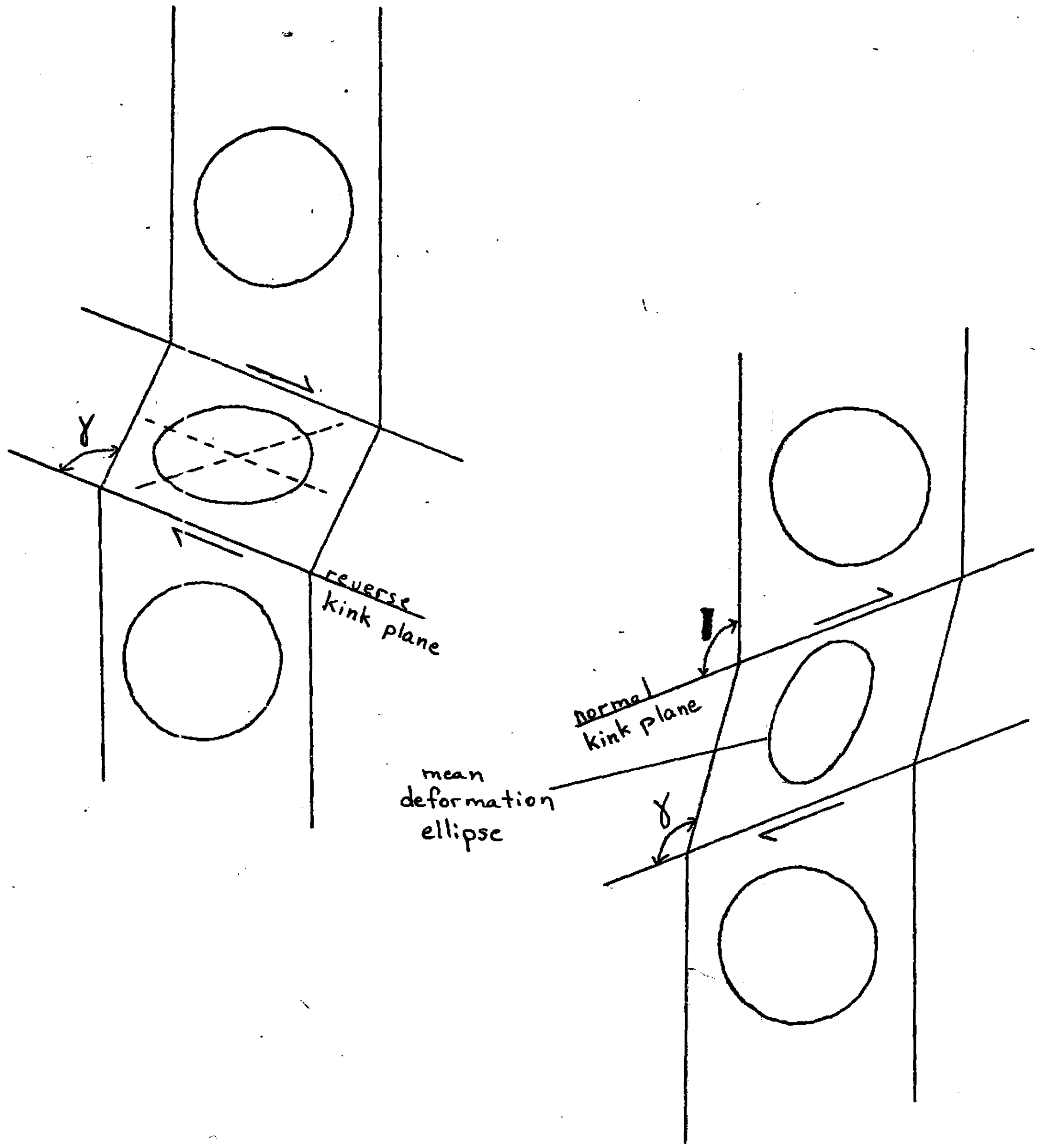

Figure 2. Terminology of kink bands.

(After Dewey, 1965)

2. Experimental Technique

In order to obtain the best results thinly rolled sheets of plasticene lubricated with talcum powder were used to model the homogeneous, anisotropic material of Biot's (1965) analysis.

Plasticene was chosen because it is reasonably uniform in composition, can be rolled thinly without seriously changing its ductility and it is ductile at the strain rate used. In order to be able to distinguish the individual layers they were of alternating black and white plasticene. The two colors of plasticene had the same properties.

Talcum powder acted as a lubricant at all boundaries. This increased the anisotropic properties of the multilayer. To achieve this effectively the powder was added just prior to the running of the experiments.

The layers were rolled to the same thickness, stacked and then cut to fit the machine (Figure 3) with the layering parallel to the z-direction. A hand-operated screw mechanism advanced the pistons which compressed the layers in the x-direction and caused them to expand in the y-direction. The side plates and end plates acted as rigid boundaries so that the boundary conditions would approximate to those assumed in the theoretical analysis.

Black and white photographs of the experiments provided a record of the progressive development of all structures produced and were used in the calculations of strain. At the end of some experiments the deformed multilayer was sectioned and photographs were taken of the new faces.

One other machine was used in the experiments (Figure 4). This machine was similar to the machine of Figure 3 except that it enabled larger layers of plasticene to be compressed.

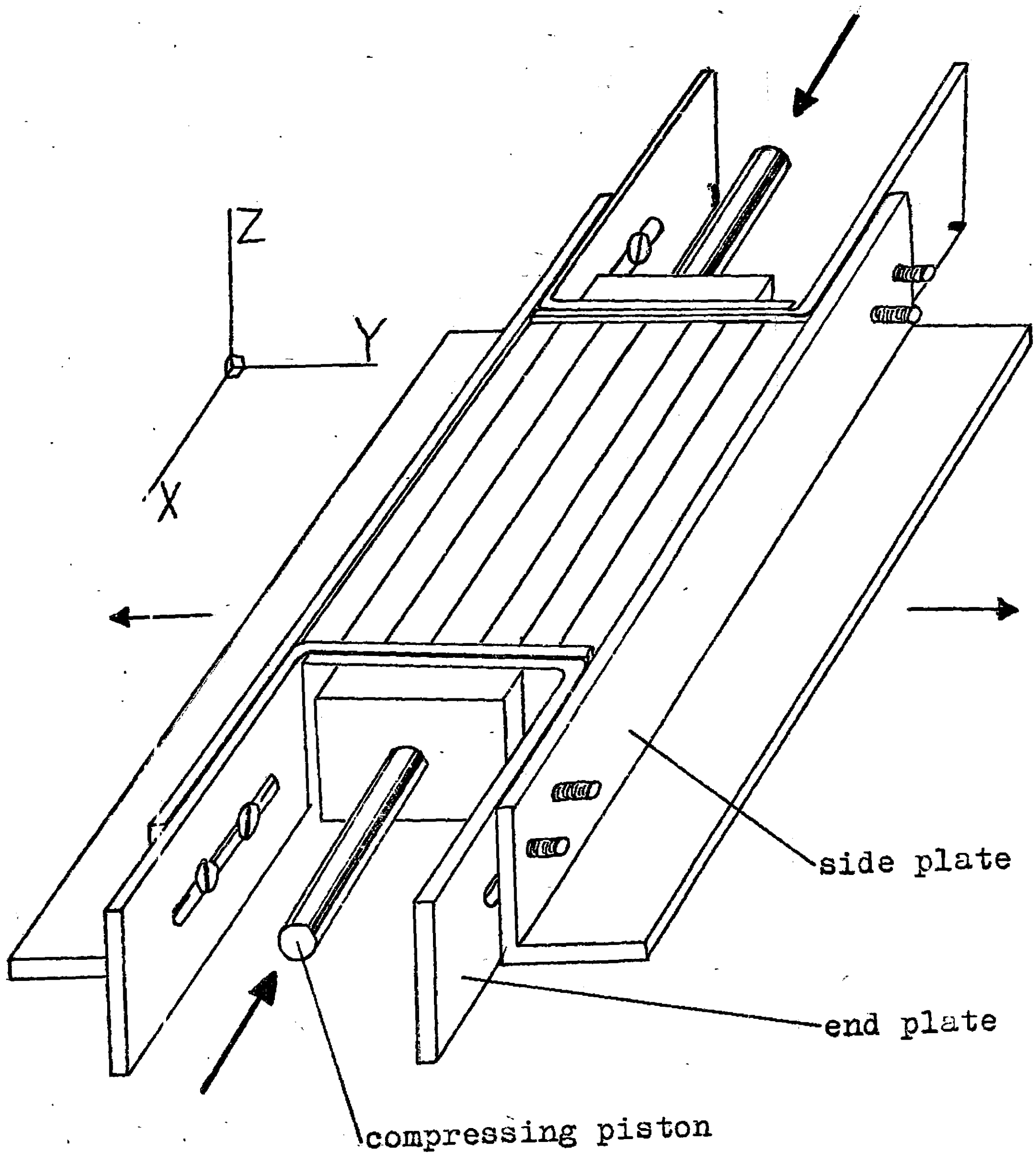

Figure 3. Machine used for deforming models.

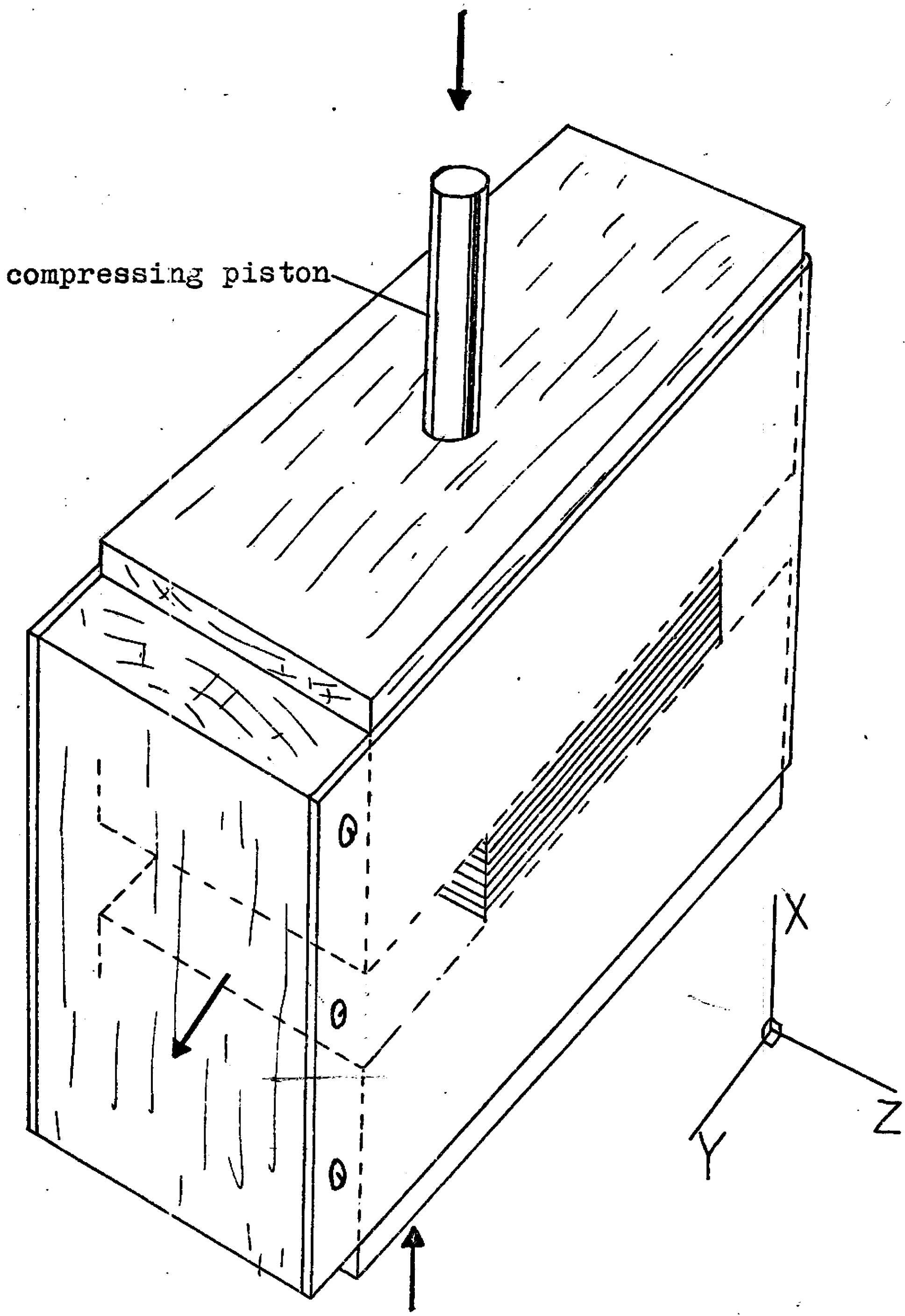

Figure 4. Machine for deforming model in experiment #6.

3. Description of Results

The original orientation of the layers, original thickness, lubricant and number of layers for each experiment are given in Table I. The orientations of the layering, the orientations of the kink bands and the per cent shortening for progressive stages of the experiments can be found in Appendix I with the photographs. The various angles describing the kink bands are shown in Figure 5 and are given in Table II for the experimental kink bands. All experiments were performed on the machine shown in Figure 3 except for experiment #6 which was performed on the machine shown in Figure 4.

Experiment #1

The layers initially compressed uniformly. At 8% shortening the layers started to buckle. The buckles formed conjugate reverse kink bands and at 18% shortening they were well developed. At 28% shortening the kink bands ceased to develop anymore and deformation continued by homogeneous flattening. At 46% shortening the experiment was terminated.

Experiment #2

Homogeneous flattening occurred until 8% shortening was achieved when conjugate reverse kink bands started to form. At 12% shortening these kink bands were well developed. At 25% shortening kink band growth ceased. Further compression only resulted in bulk shortening. The experiment was terminated after 45% shortening.

Experiment #3

Compression of the multilayer of experiment #3 resulted in homogeneous flattening until over 35% shortening was achieved. At about 40% shortening the side plates and end plates of Figure 3 came apart at one corner and this initiated a single set of normal kink bands. This kink band developed quickly and had ruptured completly to form a "shear" plane by 50% shortening. This "shear" plane was a single kink band in which the individual layers were drawn out and ruptured. This "shear" plane was originally oriented 45° to the principal compression direction but as compression continued it rotated to 50° to the principal compression direction.

Experiment #4

This experiment proceeded differently from the previous one. Upon compression one side of the multilayer rose up over the other as if a thrust sheet was being initiated. After 35% shortening this ceased and a single set of kink bands developed on the upper surface quite rapidly. The kink bands started at the two diagonal corners and grew inwards to the center of the multilayer's top surface. At 55% shortening the kink band had completely ruptured and the "shear" plane that resulted had an orientation of 50° to the principal compression direction. The resultant block of plasticene was cut as shown in Figure 40 (c)(Appendix I). Photographs were taken of the fresh surfaces and the orientations of all the "shear" planes and normal kink bands recorded.

Experiment #5

In this experiment the condition of plain strain was maintained. In order to eliminate the thrust-like sheet obtained in experiment #4 the end plates of the machine of Figure 3 were fastened to the side plates. However, they were still allowed to move freely back and forth. No features were observed on the top surface of the multilayer but when cut in the xz plane (Figure 41 (b)) well-developed conjugate normal kink bands were observed. The orientation and geometry of these kink bands were recorded.

Experiment #6

This experiment was performed in the machine shown in Figure 4. This experiment differed from the previous experiments in that the condition of plane strain was more rigorous. The layers were cut so that they occupied only half of the volume between the two blocks (therfore maximum shortening possible is 50%) and when compressed they were forced to deform by plain strain. At 25% shortening the machine was carefully dismantled to expose the multilayer. Buckling had already occurred. The machine was reassembled and shortening completed to 50%. Again the apparatus was carefully dismantled so as not to disturb the layering. Photographs were taken of all four sides of the multilayer. Plasticene had squeezed between the wood and aluminum on the two ends and partly on one side obliterating any structures. However, the other side was clear and several normal kink bands could be seen.

Experiments #7,#8,#9,#10

The rest of the experiments were performed on the machine of figure 3 with initial layering other than 90^{o} to the principal compression direction. These were run to see if the theory (section 4 (a)) can also apply to orientations other than orientations that when stressed maintained orthotropic symmetry. Experiment #7 resulted in conjugate normal kink bands, experiments #9 and #10 resulted in the development of a single reverse kink band and no kink bands developed in experiment #8 (see section 4 (d)). All the experiments were terminated after 50% bulk shortening.

TABLE I

Experimental data before deformation

Experiment number	Original orientation of layering to	Original thickness	Lubricant	Number of layers
1.	0°	3.00 mm	talcum powder	12
2.	0°	1.50 mm	talcum powder	24
3.	90°	1.50 mm	talcum powder	32
4.	90°	1.50 mm	talcum powder	48
5.	90°	1.50 mm	talcum powder	36
6.	90°	1.20 mm	talcum powder	14
7.	75°	1.50 mm	talcum powder	36
8.	60°	1.50 mm	talcum powder	42
9.	50°	1.50 mm	talcum powder	38
10.	30°	1.50 mm	talcum powder	34

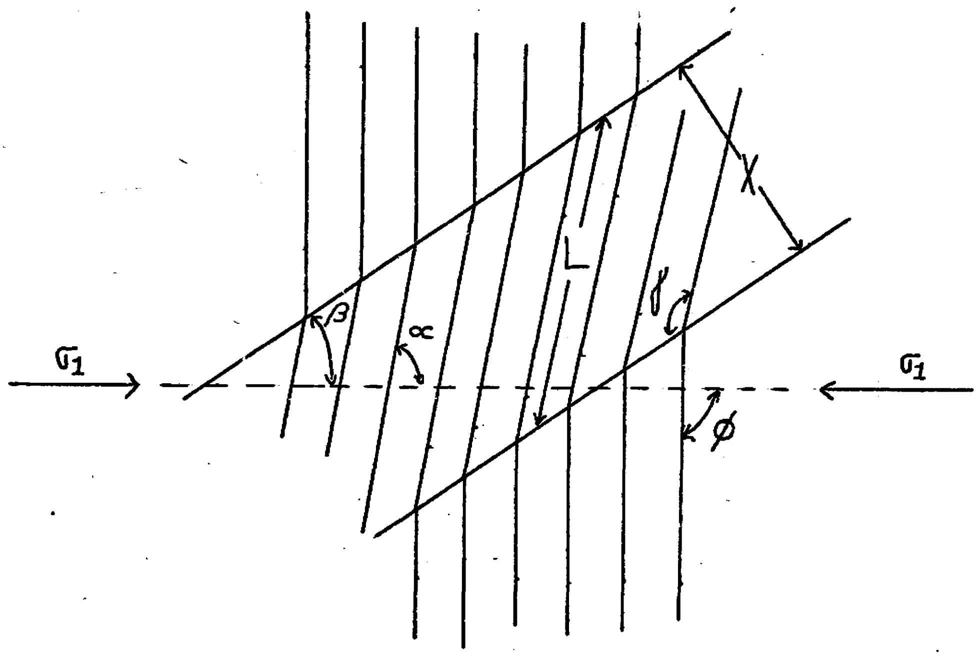

Figure 5. Angles describing the geometry of kink bands.

β is the orientation of the axial surface to the principal compression direction.

$\propto$ is the orientation of the layers in the kink band to the principal compression direction.

γ is the orientation of the axial surface to the layers in the kink band (obtuse angle).

ϕ is the orientation of the layers deformed only by homogeneous flattening to the principal compression direction.

L is the length of the layers in the kink band.

X is the width between the two axial surfaces.

TABLE II

Geometry of experimentally produced kink bands.

Experiment number	β	α	γ	ϕ	X	L
4 sec. 3	47°	76°	151°	90°	.71 cm	1.31 cm
4 sec. 4	47°	76°	151°	90°	.78 cm	1.50 cm
5 sec. 2	49°	78°	152°	90°	.68 cm	1.48 cm
5 sec. 3	50°	77°	153°	90°	.67 cm	1.26 cm
5 sec. 4	48°	76°	153°	90°	.68 cm	1.34 cm
5 sec. 5	49°	77°	149°	90°	.69 cm	1.28 cm
6	60°	—	—	90°	—	—
7 (a).	$50^{\circ},52^{\circ}$	$88^{\circ},80^{\circ}$	$141^{\circ},151^{\circ}$	81°	—	—
7 (b).	$48^{\circ},46^{\circ}$	$84^{\circ},78^{\circ}$	$144^{\circ},149^{\circ}$	85°	—	—
9	50°	72°	121°	60°	—	—
10	52°	48°	100°	33°	—	—

4. Interpretation

(a) Theory (From Biot 1965, Cobbold et.al. 1971, Cosgrove 1972)

Biot (1965) developed a deformation theory applicable to homogeneous, anisotropic material. Cosgrove (1972) applied it to the production of kink bands. The theory will not be discussed in detail here and the reader is referred to the relevant papers.

The conditions assumed in the theory are that the material is homogeneous, anisotropic, has orthotropic symmetry, is under an initial stress before instability occurs, and is deformed by plane strain. Examples of material that approximate to homogeneous, anisotropic materials are given in Cobbold et. al. (1971) and are reproduced here in Table III.

Orthotropic symmetry occurs when the layering is parallel, normal or at 45^{o} to the principal compression direction.

Let the elastic moduli of an orthotropic material be N and Q (compressive and shear moduli respectively (Biot 1965)). Let the initial stresses acting on the material be S_{11} and S_{22}. These are related to the two moduli through the stress dependent moduli M and L :

$$M = N - \frac{P}{4} \qquad \ldots\ldots 1$$

$$L = Q - \frac{P}{2} \qquad \ldots\ldots 2$$

where $P = (S_{22} - S_{11})$(Biot 1965, p.194). The moduli M and L are useful because they simplify many mathematical equations and are experimentally measurable quantities. The relationships have viscous and elastic-viscous analogues. The orthotropic orientations are important. These are the only orientations for which the theory predicts structures. However, it can generally apply to other orientations as will be shown later.

A convenient measure of the anisotropy of a material is the ratio of the two moduli M and L. When M and L are very different the material has a high degree of anisotropy.

The buckling equation for theoretical material contains the moduli M and L and shows that the displacement associated with buckling depends upon the moduli (Biot 1965):

$$(L - P)\frac{\partial^4 \psi}{\partial x^4} - 2\,(M - L)\,\frac{\partial^4 \psi}{\partial x^2 \partial y^2} - L\,\frac{\partial^4 \psi}{\partial y^4} = 0 \qquad \ldots\ldots 3$$

The general solution of the above equation is (Biot 1965, p.195):

$$\psi = f_1(x + \xi_1 y) + f_2(x - \xi_1 y) + f_3(x + \xi_2 y) + f_4(x - \xi_2 y) \ldots\ldots 4$$

where ξ_1 and ξ_2 are arbitrary constants and f_1, f_2, f_3 and f_4

are any arbitrary functions. ξ_1 and ξ_2 can be either real or imaginary. Only the real values are of interest to us. Real values of ξ_1 and ξ_2 exist in the following cases (Cosgrove 1972) :

1. $\frac{M}{L} > \frac{1}{2}$; $\frac{P}{L} > 1$
2. $\frac{M}{L} < \frac{1}{2}$; $1 > \frac{P}{L} > 4 \left(\frac{M}{L} \left(1 - \frac{M}{L} \right) \right)$
3. $\frac{M}{L} < \frac{1}{2}$; $\frac{P}{L} > 1$

These three cases correspond to three types of instabilities, Type I, Type II, and Type III (Figure 6).

Type I and Type III instabilities are alike. Type III is rarely seen because it is energetically the least favourable instability for deforming the material. The Type II instability field is reached before the Type III instability field.

The displacement equation for Type I instability was obtained and it ~~was~~ found that the displacement pattern causes an initially rectangular grid parallel to the x and y directions to vary sinusoidally with wavelengths λ_x and λ_y along the coordinate directions x and y respectively (Figure 7).

Choosing a particular type of equation (Biot 1965, p.195)

$$\psi = -C \cos lx \cos \xi ly \qquad \text{...... 5}$$

where C is an arbitrary constant it is found that the parameter ξ is equal to the ratios of λ_x and λ_y. M and L are functions of the initial stress P. If the biharmonic equation is rewritten with the above equation substituted for ψ:

$$P = L\xi^4 + 2(2M-L)\xi^2 + L \qquad \text{...... 6}$$

it is seen that there is an implicit relation between ξ and P (Biot 1965,p.196)(Figure 8). Compressive stresses of magnitude less than L are insufficient to cause internal buckling of Type I instability and it follows that the most easily formed displacement pattern occurs when $P_{CRIT} = L$. This corresponds to a value of 0 for ξ. As pointed out by Biot (1965) " the results indicate that the buckling tends to occur with the shortest possible wavelength compatible with the small scale geometry of the layers and their rigidity contrast. The buckling wavelength is then governed by additional factors such as the layer thickness, which cause a departure from the behaviour of the continuous model derived ..."(p.199). Biot's first statement indicates that if the wavelengths are small the directions that disturbances within the material tend to propagate along, characteristic directions, are approximately at 90° to the principal compression direction.

This relatioship can be seen in some experiments, eg. by comparing experiments #1 and #2 (Figures 38 and 39) it can be seen that the buckles in experiment #1 are larger than in experiment #2. The thinner the layers the closer the multilayer will approximate to the theoretical model. The wavelegths are a function of the layer thickness.

Type II instability occurs along characteristic directions that are oblique to the y-direction as opposed to Type I where the instabilities develop parallel to the y-direction. The orientations of the characteristic directions are shown in Figure 9 and depend on the ratio of the moduli M and L , which is a measure of the degree of anisotropy of the material. A material with a high degree of anisotropy will have the characteristic directions $\pm 45^{\circ}$ to the y-axis and a material with a lower degree of anisotropy will have characteristic directions at angles less than 45°.

The theory says nothing about the form of Type II instabilities. Experiments, however, indicate that a Type II instability when developed in layered material may be expressed as kink bands with the bands oriented along the characteristic directions.

An important fact about kink band formation can be brought out at this point. Consider a multilayer made up of perfectly parallel layers, with no irregularities, being compressed perpendicular to the layers. They will deform by bulk shortening until the critical state when $P_{CRIT} = L$. If L is low, for example cohesion between the layers low, the ratio $\frac{M}{L}$ is very high. Therefore, when $P_{CRIT} = L$ the layers will develop Type I instabilities. This causes a deviation from parallelism and the resistance to compression M, parallel to the x-direction becomes the resistance to slip (L) between the layers. This "inversion" (Cobbold et. al. 1971) causes the $\frac{M}{L}$ ratio to become less than $\frac{1}{2}$ at the points of perturbation and Type II instabilities may develop. When slip between layers occurs the disturbance is propagated into the surrounding area and the area of instability grows. Although kink bands should only occur in materials with $\frac{M}{L} < \frac{1}{2}$ they can start in materials with $\frac{M}{L} > \frac{1}{2}$ by the development of internal boudins which may grow into kink bands along characteristic directions (Figure 10).

Type I and Type III instabilities will develop in materials with $\frac{P}{L} > 1$. Type II instability will develop in materials with $0 < \frac{M}{L} < \frac{1}{2}$, $\frac{P}{L} < 1$ and so will develop before Type III instability. Type I and Type III instabilties are associated with sinusoidal buckling whereas Type II is associated with kink band development along characteristic directions oblique to the y-direction. The forms of the instabilities are dependent on the orientation of the layers as wellas the degree of anisotropy. (Figure 11)

TABLE III

Some examples of materials that are statistically homogeneous

---

1) A stack of layers with alternating competences and with cohesion at the layer boundaries.

2) A stack of layers of the same material, but with discontinuities at the layer boundaries.

3) A composite material with a fabric of parallel planar elements but not necessarily with continuous layers.

4) A bundle of continuous, parallel rods, with no cohesion between them.

5) A composite material with a fabric of parallel linear elements.

Some geological examples:

Regularly alternating shales, sandstones and greywackes

Well-bedded limestones

Varved evaporites

Banded gneisses

Rocks with tectonically induced mineral banding

Banded rhyolites

Layered gabbros

S-tectonites

Gneisses with flat augen

Schists

Phyllites and slates

L-tectonites such as amphibolites or rodded gneiss

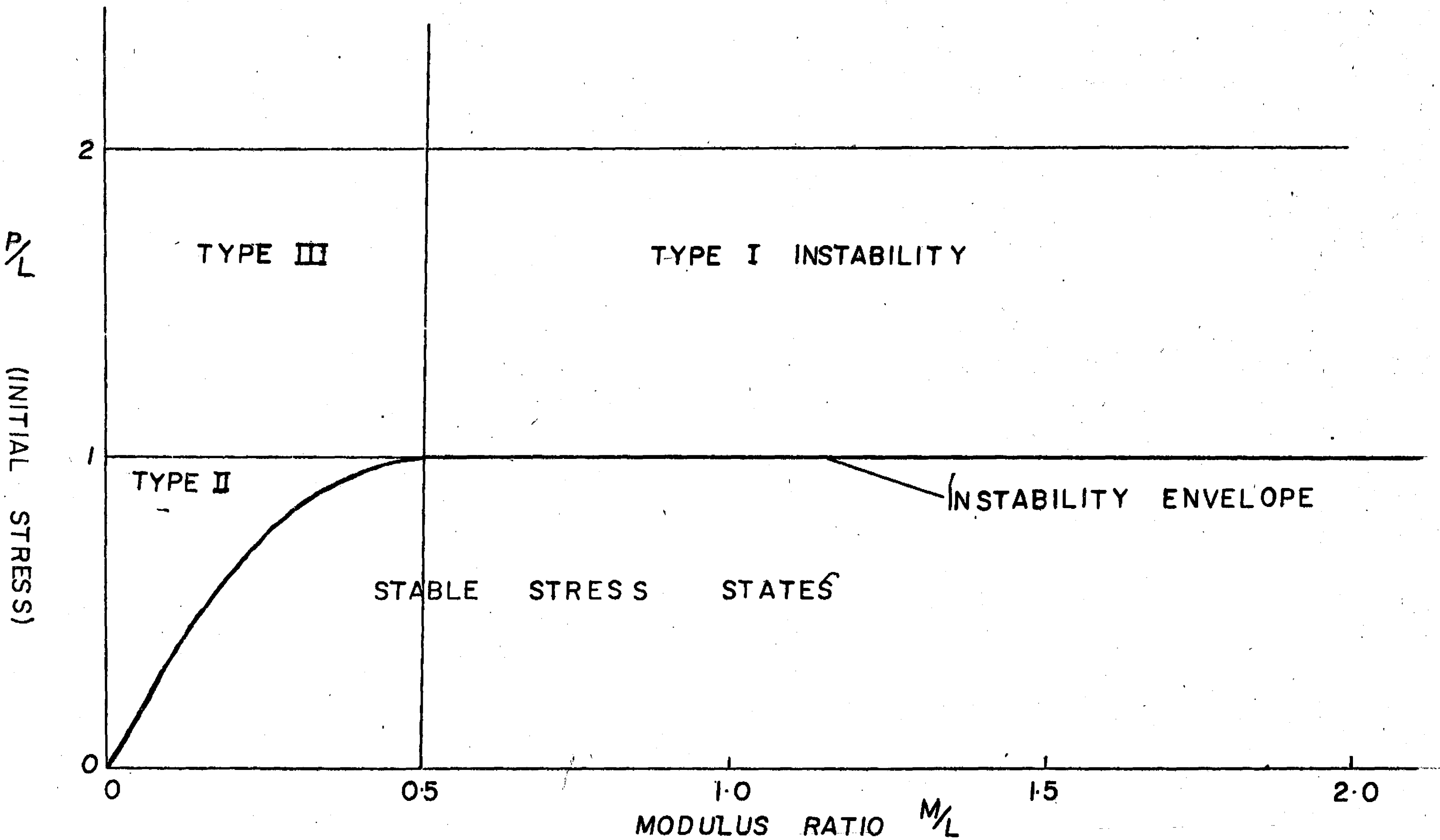

Figure 6. Stable and unstable values of the initial stress, P, in materials with different degrees of anisotropy. The thick black line represents the critical stress P_c of eq. 6.

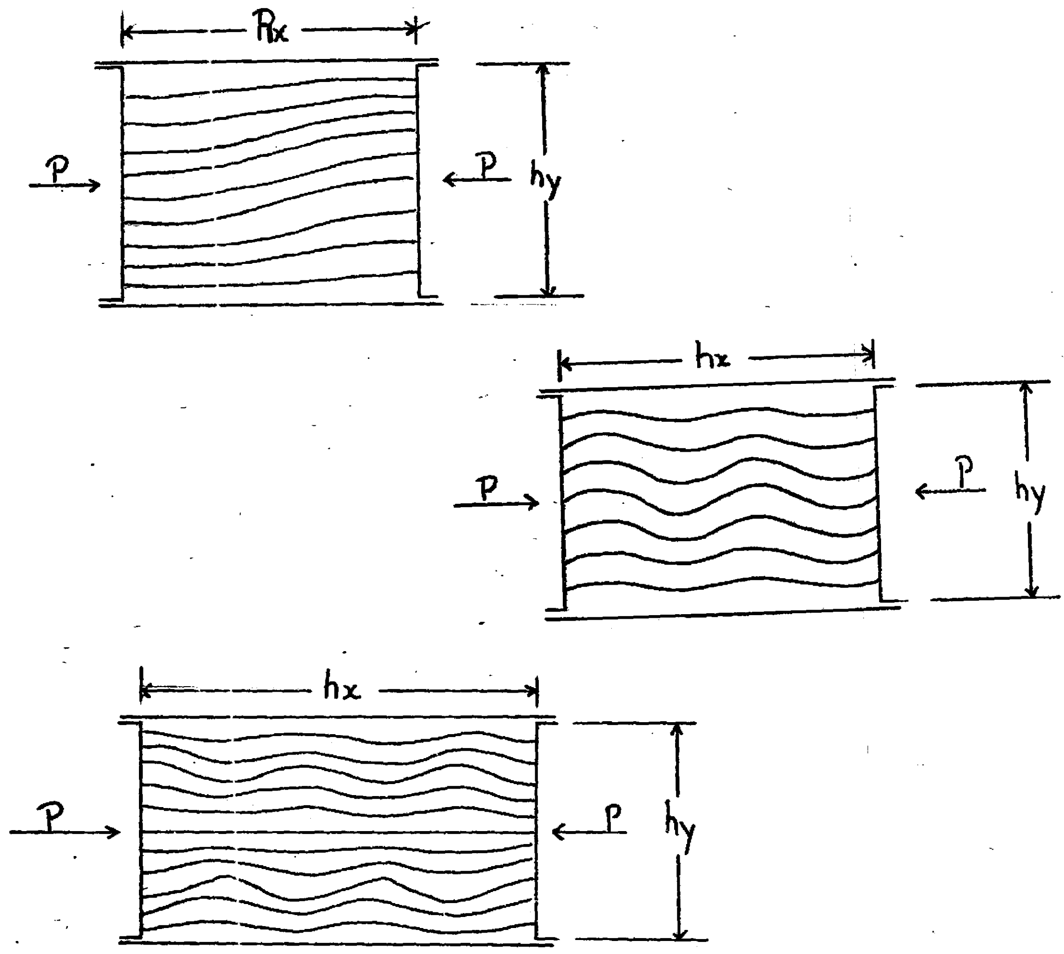

Figure 7. Various forms of Type I instability.

(From Biot, 1965)

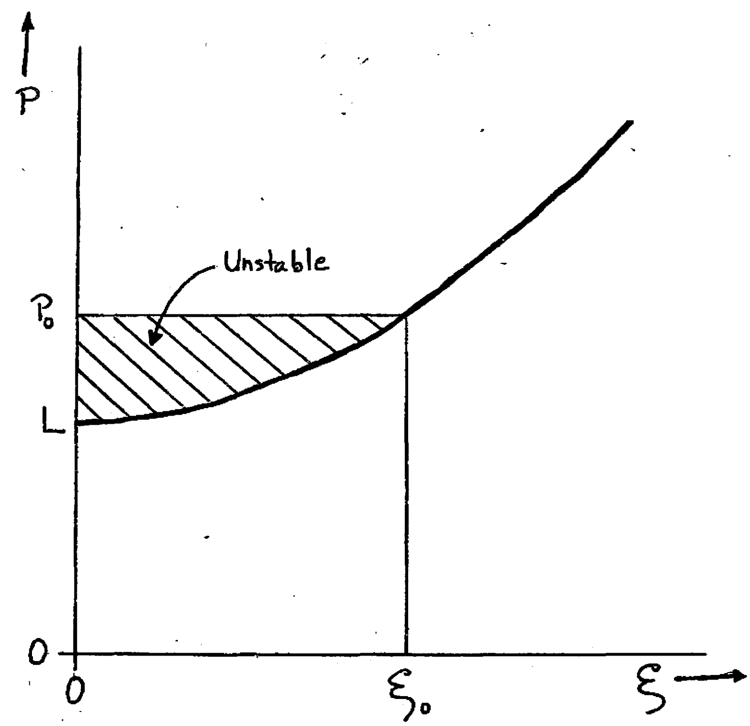

Figure 8. Diagram for internal instability of Type I.

(From Biot 1965,p.196)

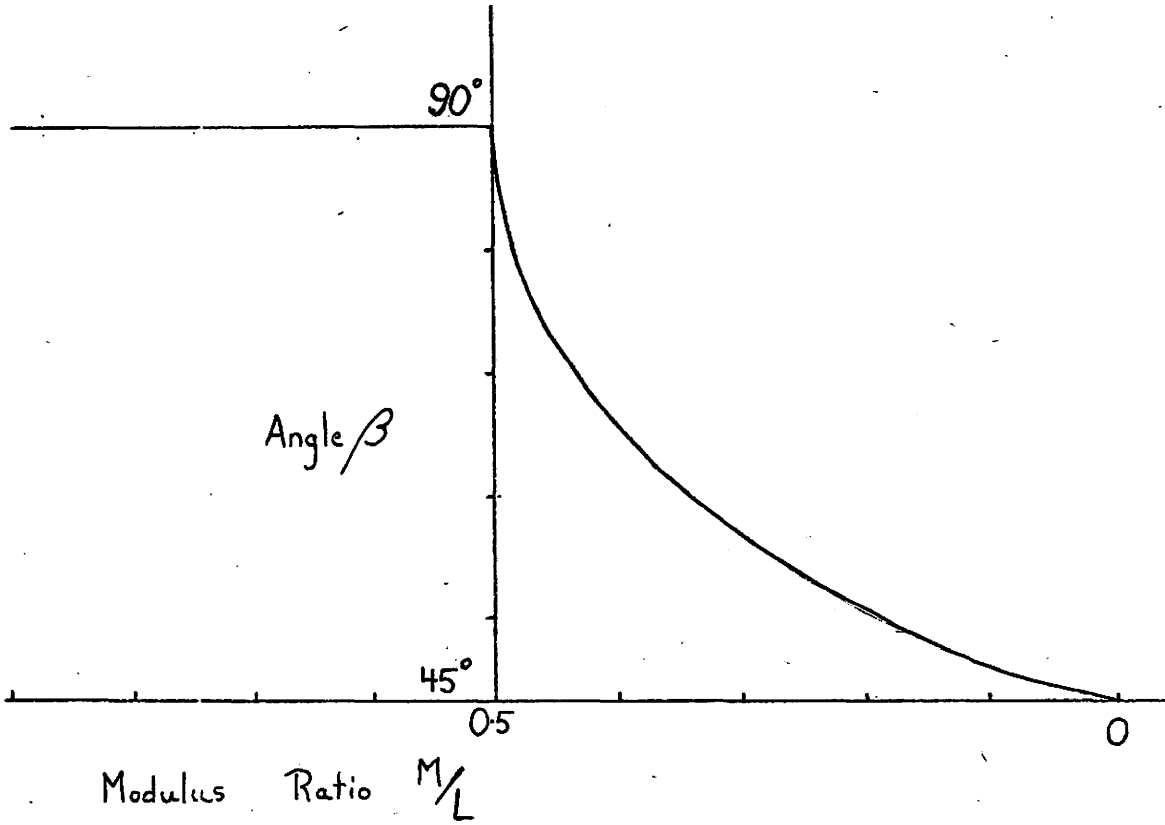

Figure 9. Orientation of the Characteristic Direction for various $\frac{M}{L}$ values. β is measured from the compression direction.

(From Cosgrove 1972)

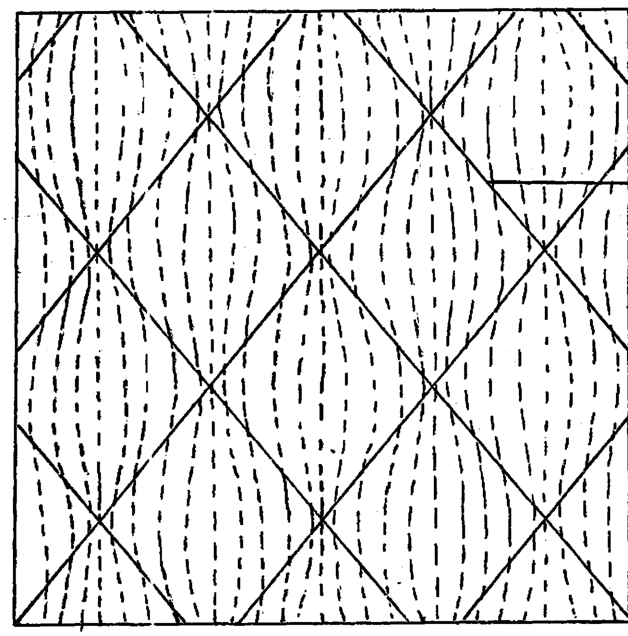

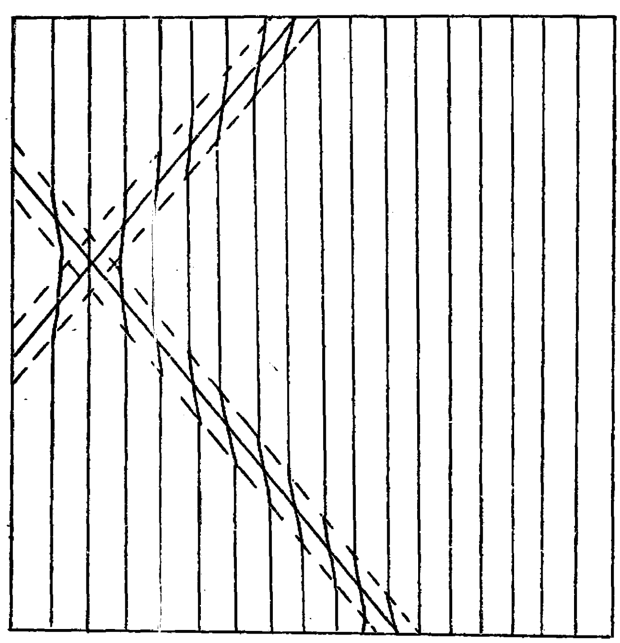

Figure 10. Development of kink bands from Type I instability.

(After Cosgrove,1972)

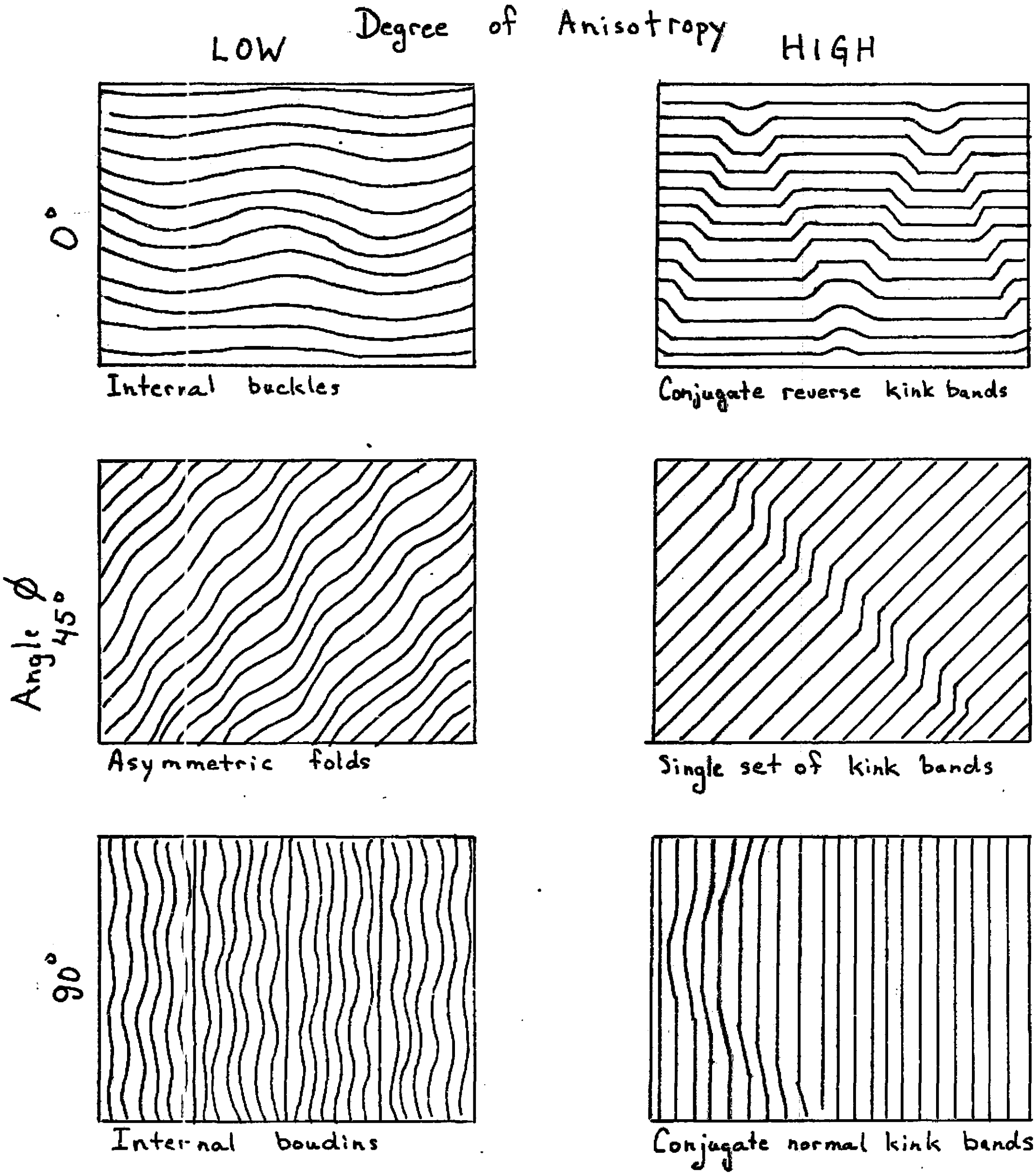

Figure 11. Summary of the combined effects of degree of anisotropy and orientation of layering on the form of internal fold structures which might develop in a statistically homogeneous rock. The angle ∅ is that between the compression direction and the layering.

(After Cobbold et. al., 1971)

(b) Orientation of stress axes

In the theoretical analysis it was assumed that the principal compression direction (σ_1) was parallel to the x-direction and the expansion direction (σ_3) parallel to the y-direction. The material was subjected to plane strain. The buckling instabilities developed in the xy plane.

In the experiments it is found when the principal compression was applied parallel to the x-direction the other directions (y or z) may be either σ_2 or σ_3. As a result of this the instabilities sometimes developed in the xz plane (experiment #5), sometimes in the xy plane (experiment #3) and sometimes in both (experiment #4).

In experiment #4 one side rode up over the other as if a thrust was being generated. Following this a normal kink band developed on the top of the multilayer. Serial sectioning of the deformed block enabled the history of the deformation to be deduced. Conjugate normal kink bands developed in the xz plane. One of the normal kink bands developed much faster than the other (Figure 12a). This kink band developed rapidly and ruptured. One side of the multilayer then slid up over the other (Figure 12b). The compressing end plate caught the "foot wall" and further slip on the "shear" plane was suppressed and compression started again. This caused a normal kink band to form in the "foot wall" section but because it was cut off from the "hanging wall" section it failed to propagate across the "shear" zone (Figure 12c). Meanwhile compression was being applied to the "hanging wall" section. This caused a normal kink band to form on the xy plane. Again the kink band did not propagate across the "shear" zone which acted as a "barrier"(Figure 12d).

At the start of experiment #4 the σ_3 direction was vertical (z directed) instead of horizontal (y directed). This caused kink bands to form in the xz plane. The orientation of σ_3 in the "foot wall" section remained constant but as soon as the vertical movement of the "hanging wall" ceased the σ_3 direction in the "hanging wall" changed to horizontal (y directed). This caused kink bands to form on the xy plane. However these kink bands were restricted to the "hanging wall" and did not propagate over the "shear" plane into the "foot wall".

In order for this interchange of stress directions to occur σ_2 must be approximately equal to σ_3 but <u>not</u> equal to σ_1 (i.e. $\sigma_1 > \sigma_2 \doteq \sigma_3$)

In experiment #3 no kink bands occured in the xz plane so σ_3 must have remained parallel to the y-direction throughout the experiment.

In experiment #5 the kink bands formed on the xz plane, not the xy plane. During deformation no kink bands were seen on the top surface (xy surface) but when it was sectioned kink bands were observed in the vertical position (xz plane). These kink bands were the same throughout the multilayer (see section 4 (c)) and were the only kink bands observed. If kink bands form on the $\sigma_1\sigma_3$ plane then the z-direction on the machine must have been parallel to σ_3.

In the theory it is assumed that the x-direction is parallel to σ_1 and the y-direction is parallel to the σ_3 direction and the obtuse angle subtended by conjugate kink bands is bisected by the σ_1 (x) direction. In the theory, under plane strain the principal stress directions are parallel to the strain directions. However, experimentally it was found that the σ_3 direction was not related to the y-direction. It could take up any orientation in the zy plane. To conclude from this the stress field applied by the machine is of the form $\sigma_1 > \sigma_2 \doteq \sigma_3$ i.e. prolate ellipsoidal. This may be important geologically and will be discussed later.

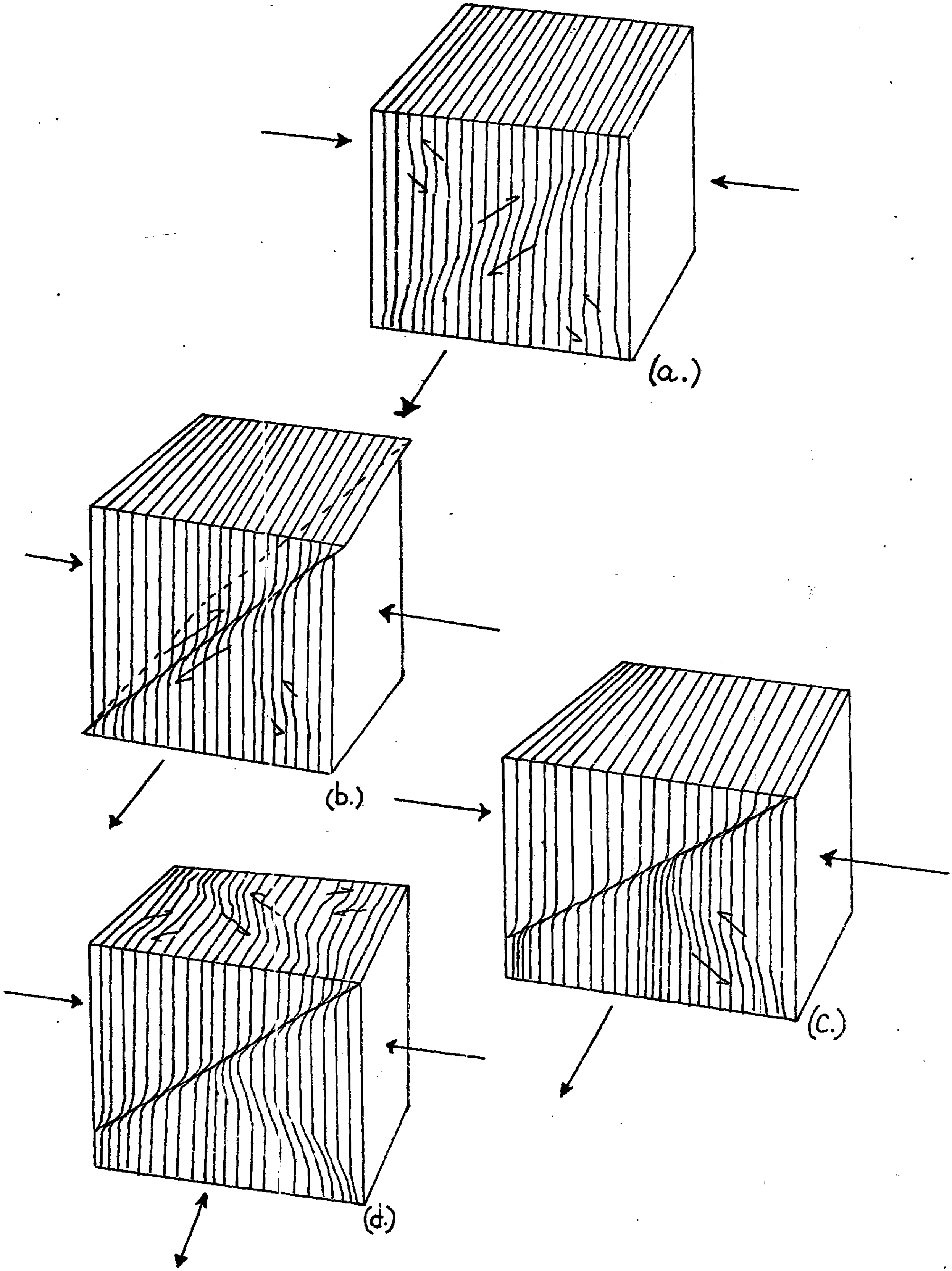

Figure 12. Progression of experiment #4 with continual compression.

(c) Geometry of kink bands produced experimentally

The kink bands produced in experiments #4, #5, #7, #9 and #10 were subjected to geometric analysis. The various parameters measured are given in Figure 5. The values for each kink band are noted in Table II and shown along with their photographs in Figures 13 to 22.

Figures 13 to 18 have the same angle orientations so that apart from their X and L values they can be readily compared. The average value of β is 49° which if compared with Figure 9 from Cosgrove (1972) gives a value for $\frac{M}{L}$ of 0.17 during the Type II instability. If the Type II instability followed Type I instability then the $\frac{M}{L}$ value in the unstrained state was 5.89. From the similarity of β it follows that the α and γ values should be the same for these experiments.

Experiment #6 was run on a different machine (Figure 4). There was no restriction on movement of plasticene in the y-direction and kink bands appeared on the xy plane ($\sigma_1 \sigma_3$). Since a larger multilayer was used than in experiments #3, #4 and #5 more conjugate kink bands were formed. The angle of the kink band axial plane (characteristic direction)(β) was recorded (Table II).

The characteristic direction was 60°. This gives the $\frac{M}{L}$ ratio a value of 0.34 which is higher than in experiments #3, #4 and #5. The anisotropy of the multilayer of experiment #6, which was made less than in experiments #3, #4 and #5, made the characteristic direction change (i.e. the orientation of the kink bands). It follows that the orientation of the characteristic directions is a function of the anisotropy (Figure 9). It should be noted that due to the lower anisotropy not only normal kink bands formed but pinch-and-swell features (Figure 23) also.

In experiments #7, #9 and #10 the ϕ values were varied and as a result the values of the other angles changed with each experiment. The β angle, which gives the degree of anisotropy, is higher than in the previous experiments where $\phi = 90^{\circ}$. This shows that the degree of anisotropy is a function of the orientation of the layers to the principal compression direction (Figure 35) with the highest degree of anisotropy being the orthoropic orientations where there is the greatest difference between the two moduli M and L.

Measurement on the variation of layer thickness provided an adequate description of the kink bands (Figures 24 to 30) because these variations followed the general outline of the kink bands quite well. Since the original thickness of the layers was known the strains were calculated and their relatioships to the contours noted (Table IV).

The multilayer deformed homogeneously until the instabilities started. At this point the multilayer deformed heterogeneously. Dewey (1965) pointed out that in angular kink band formation the strain pattern produced between the two bounding planes is homogeneous and outside the kink bands the only deformation that would take place is homogeneous flattening. As the layers within the kink bands approximate to folds the strain gets more heterogeneous between the bounding planes.

From the strain patterns constructed it can be seen that the strain within the kink bands is not homogeneous. Also in the region outside the kink bands the layers have defomed heterogeneously. Inspection of Figures 24 to 30 reveals several interesting facts. The highest negative strains (compression) are found at the intersection of the conjugate normal kink bands. On the four sides bounding the multilayer there are areas of positive strain (expansion).

The direct consequence of strain is material reallocation. It was **therefore** necessary to see how the material was redistributed during the formation of the normal kink bands.

The general form and size of the kink bands did not change in the σ_2 direction and from direct evidence it was seen that the material from one layer wasn't transported to the adjacent layers. Also, the areas of the individual layers in the $\sigma_1\sigma_3$ plane were the same (Figure 31). The material redistribution then only occurred in the $\sigma_1\sigma_3$ plane in the individual layers, and the rectangular boundaries were always maintained.

The result is that material flowed along the layers from the center of the multilayer towards the boundaries. This accounts for the thinning of layers in the middle and the widening near the two boundaries. A thickening of the layers occurred at the other two boundaries as a result of material flowing from the kink bands into the center of the layers (Figure 32). This is a consequence of the high ductility of plasticene at the strain rate used. Normal kink bands in rocks should be studied to determine their elastic formation.

The effect of material redistribution is kept at a minimum with small X and L values. The limit would be $X = L = 0$ and there would be no material redistribution. In this case the instability would be expressed as a type of faulting, the fault plane corresponding to the characteristic directions.

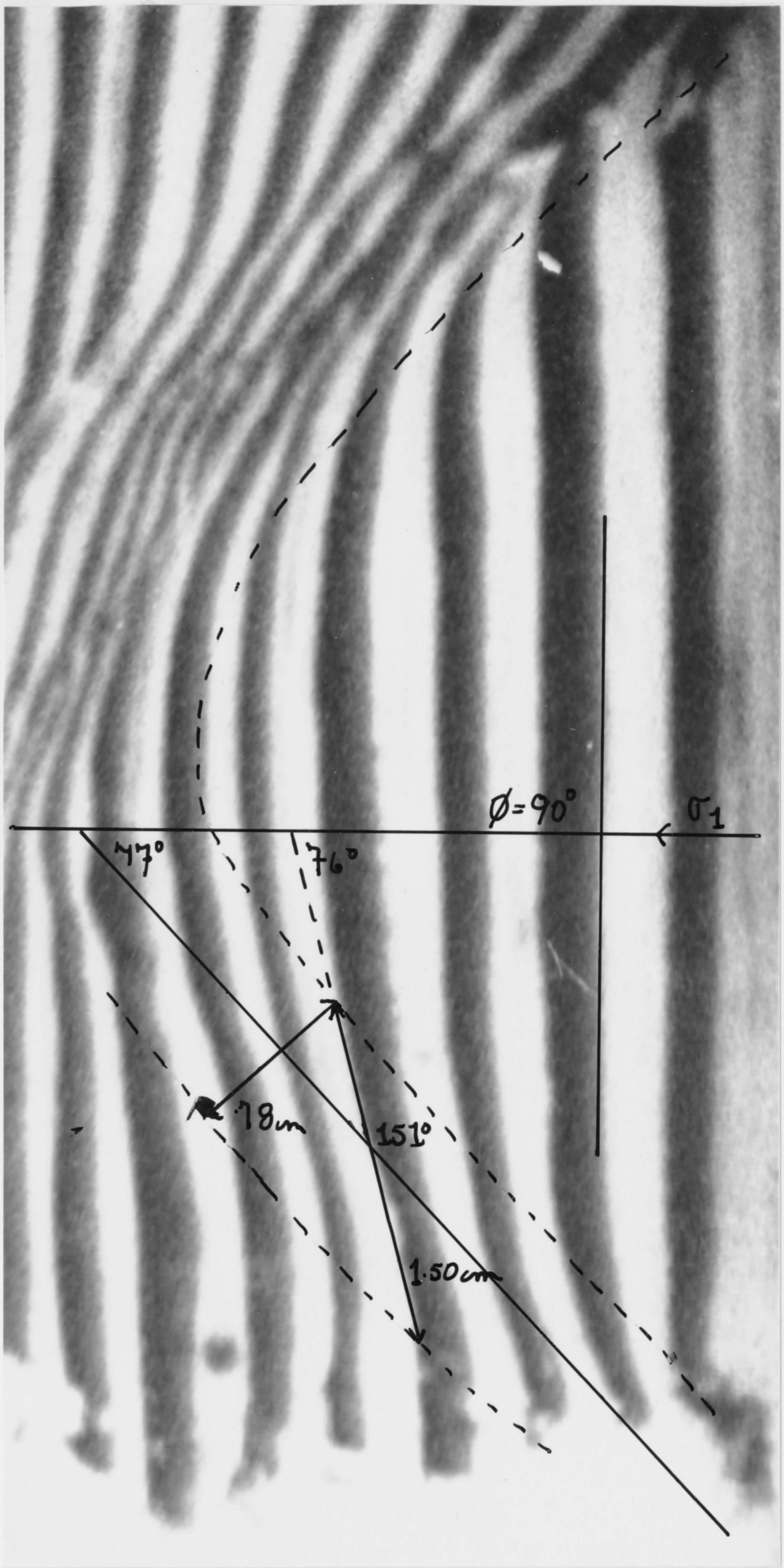

Figure 13. Photograph of Experiment #4, section 3, showing measured parameters.

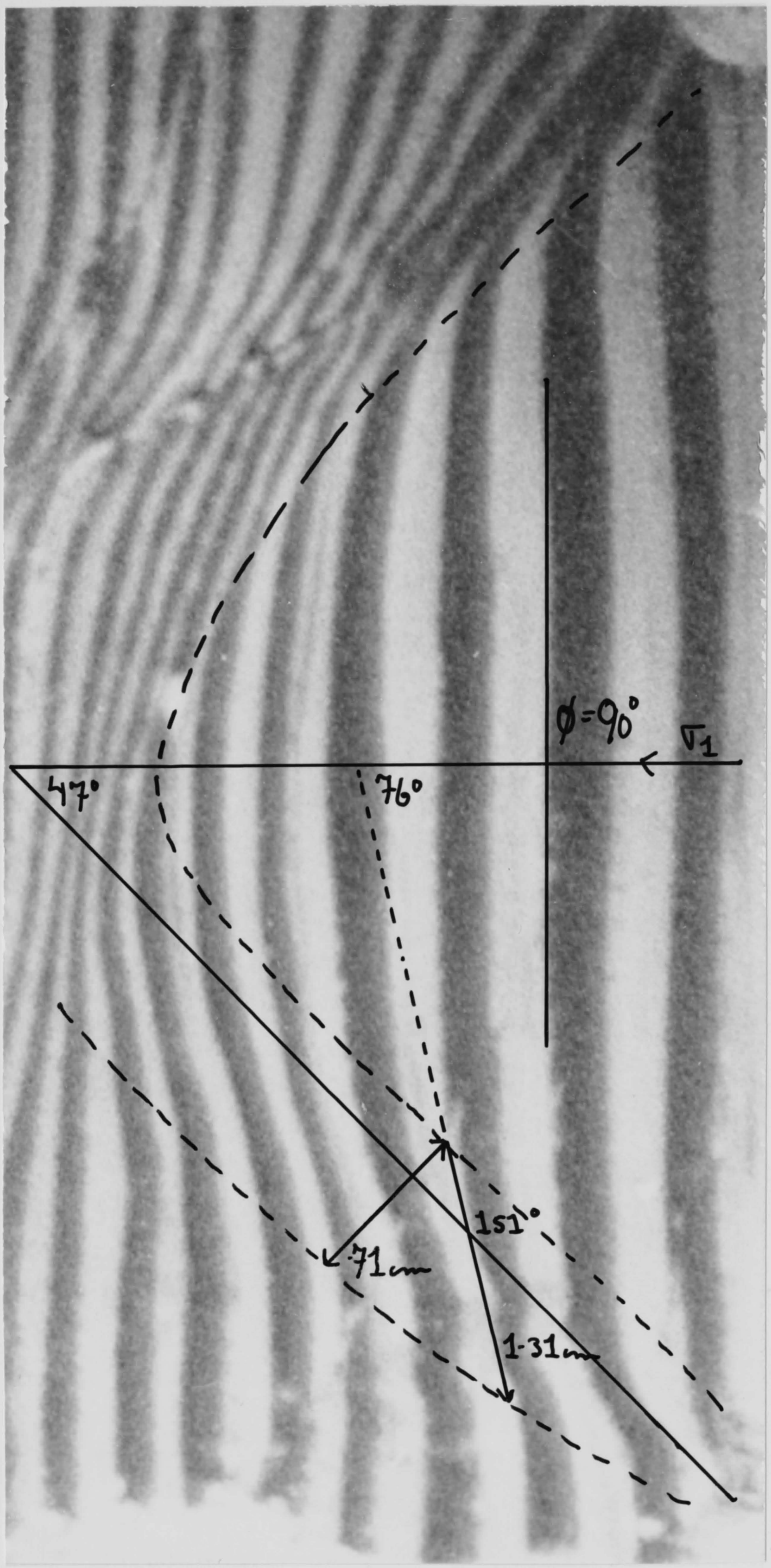

Figure 14. Photograph of Experiment #4, section 4, showing measured parameters.

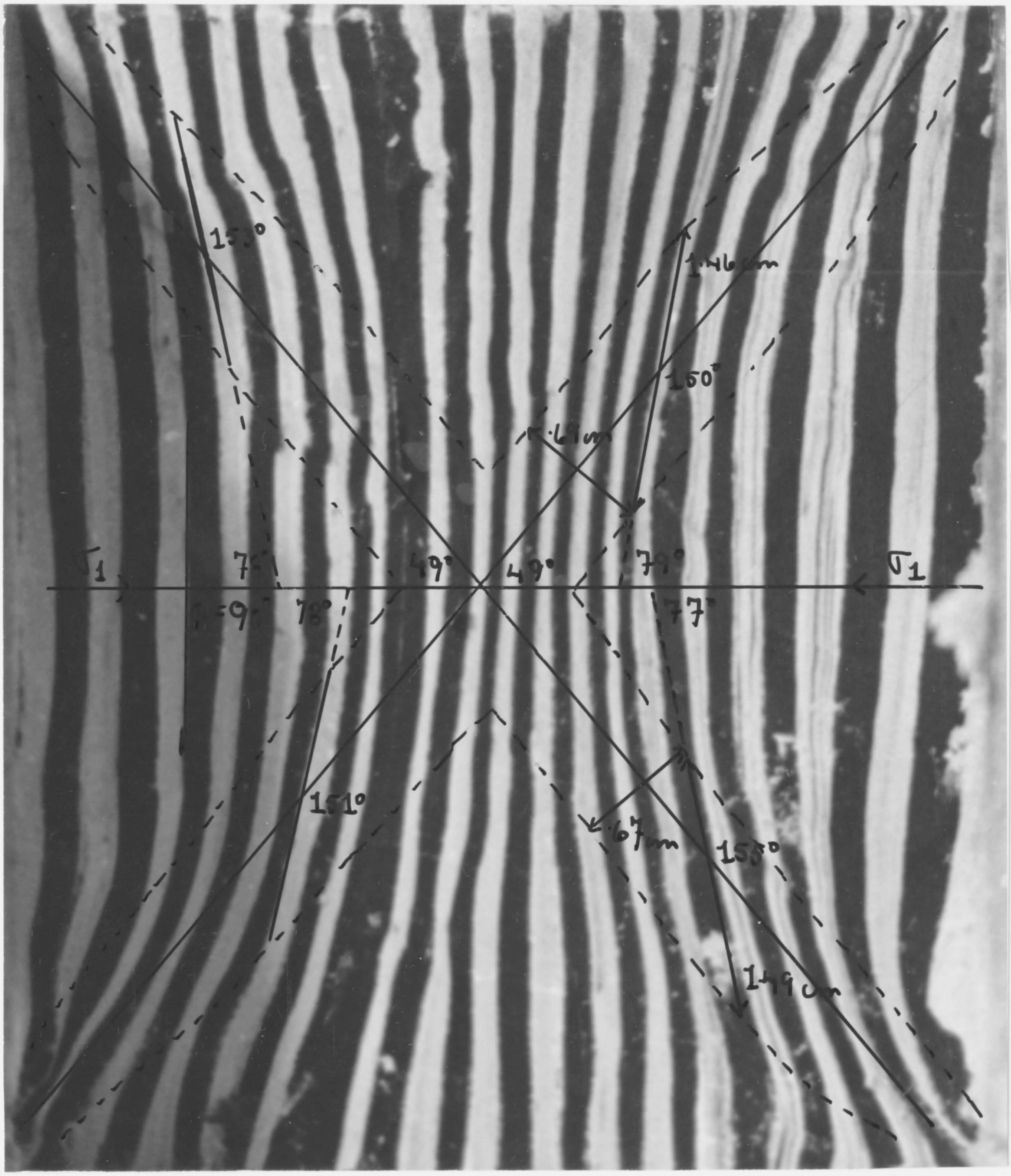

Figure 15. Photograph of Experiment #5, section 2, showing measured parameters.

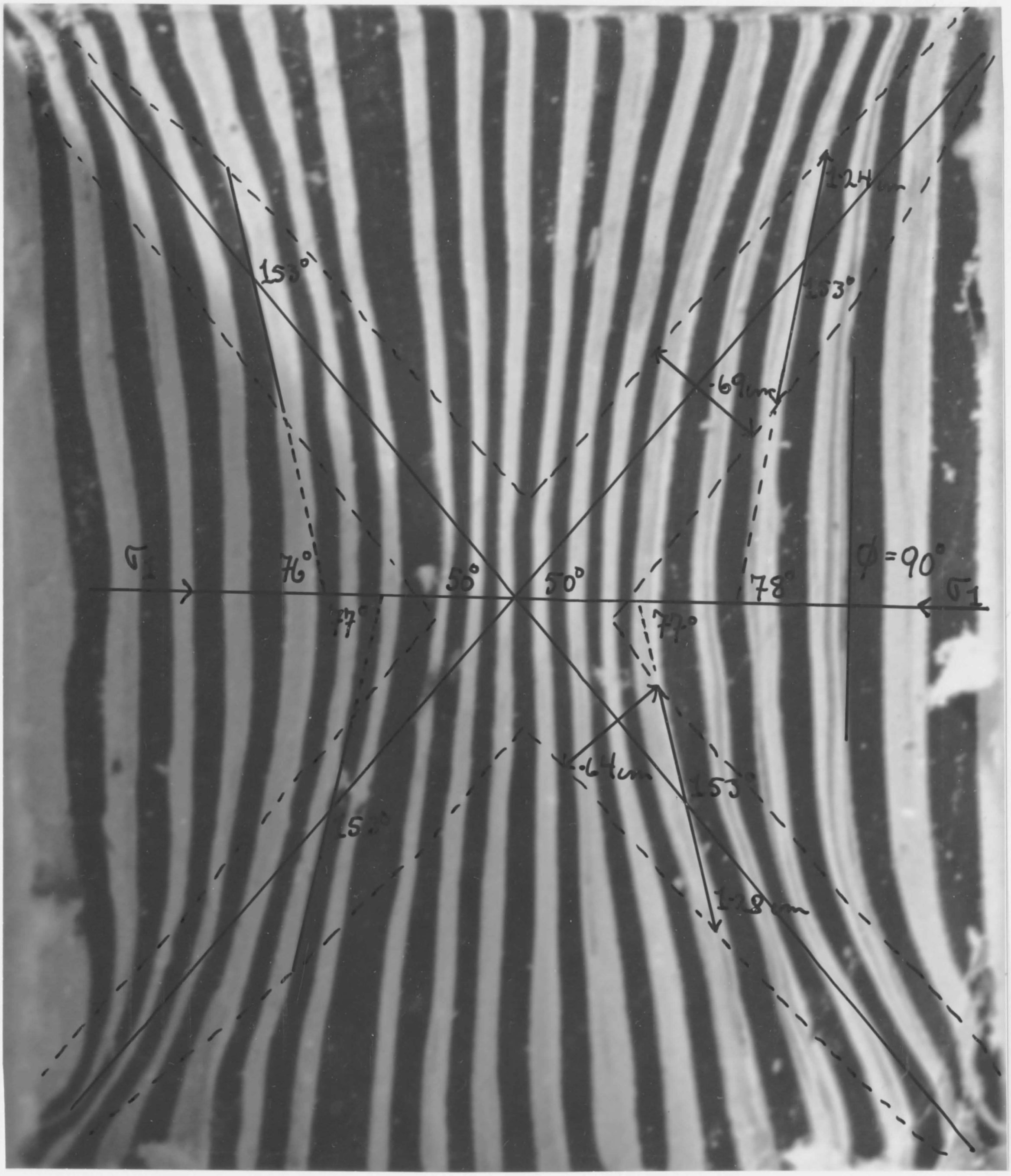

Figure 16. Photograph of Experiment #5, section 3, showing measured parameters.

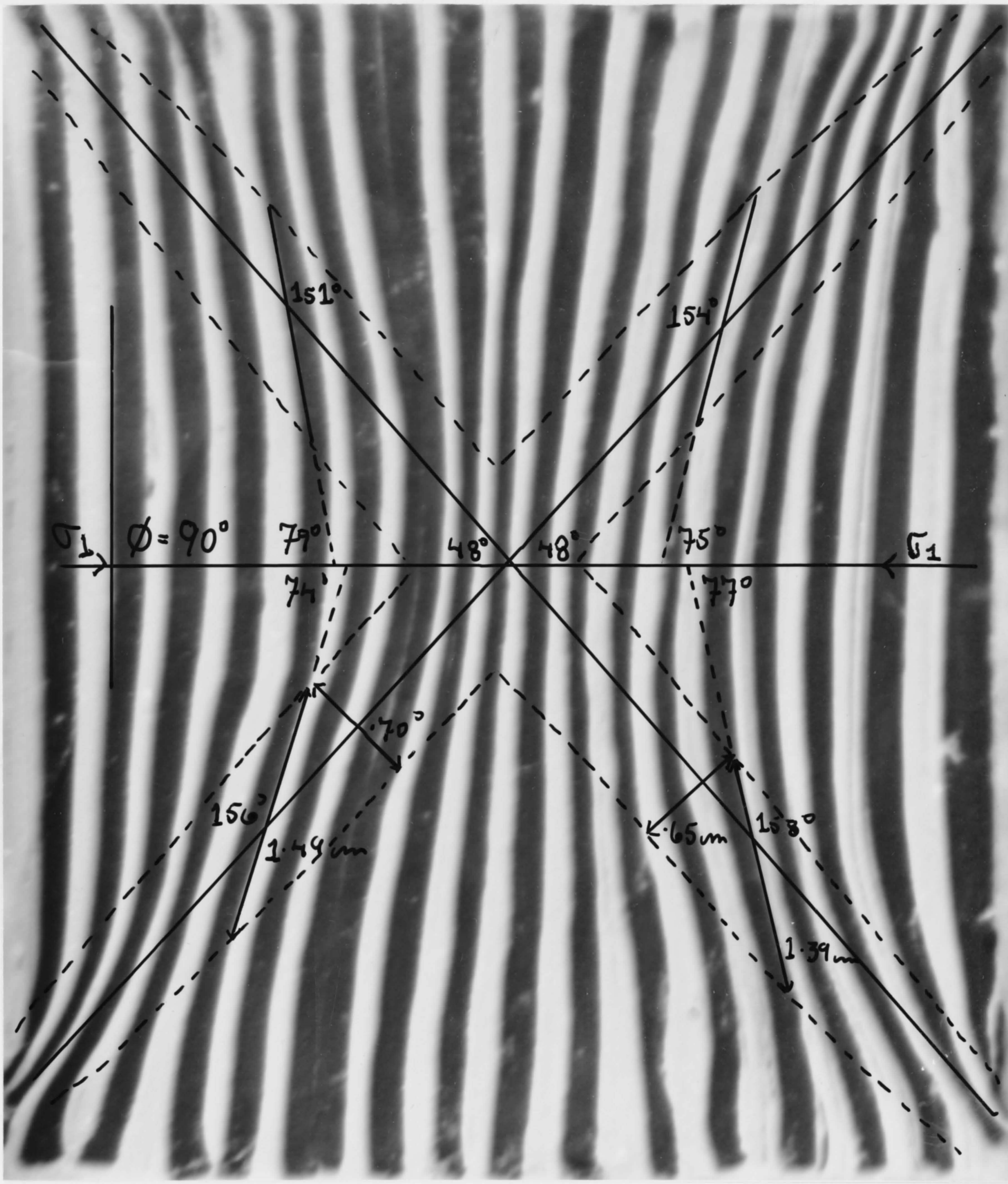

Figure 17. Photograph of Experiment #5, section 4, showing measured parameters.

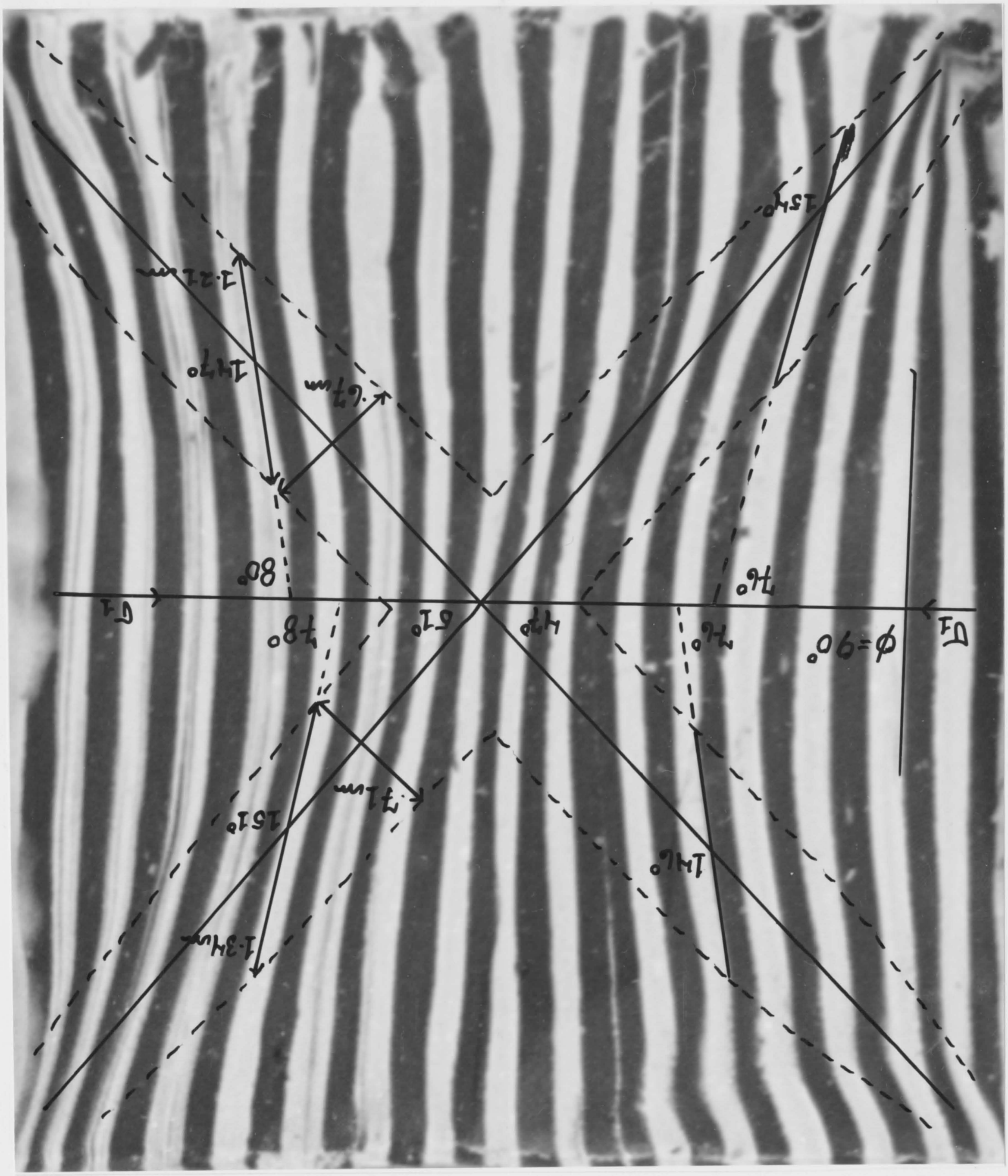

Figure 18. Photograph of Experiment #5, section 5, showing measured parameters.

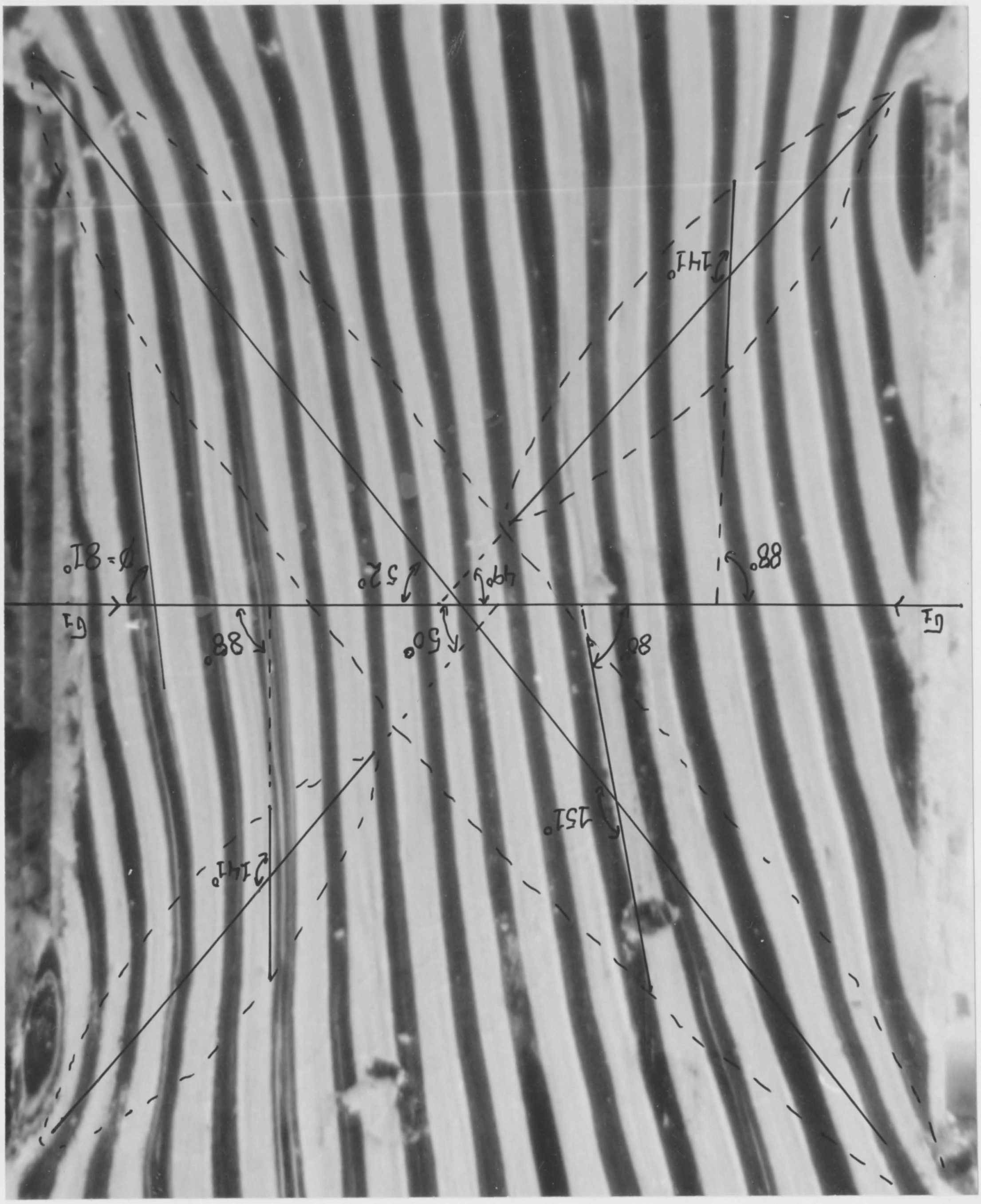

Figure 19. Photograph of Experiment #7 (a) (50% shortening) showing measured parameters.

Figure 20. Photograph of Experiment #7 (b) (55% shortening) showing measured parameters.

Figure 21. Photograph of Experiment #9 showing measured parameters.

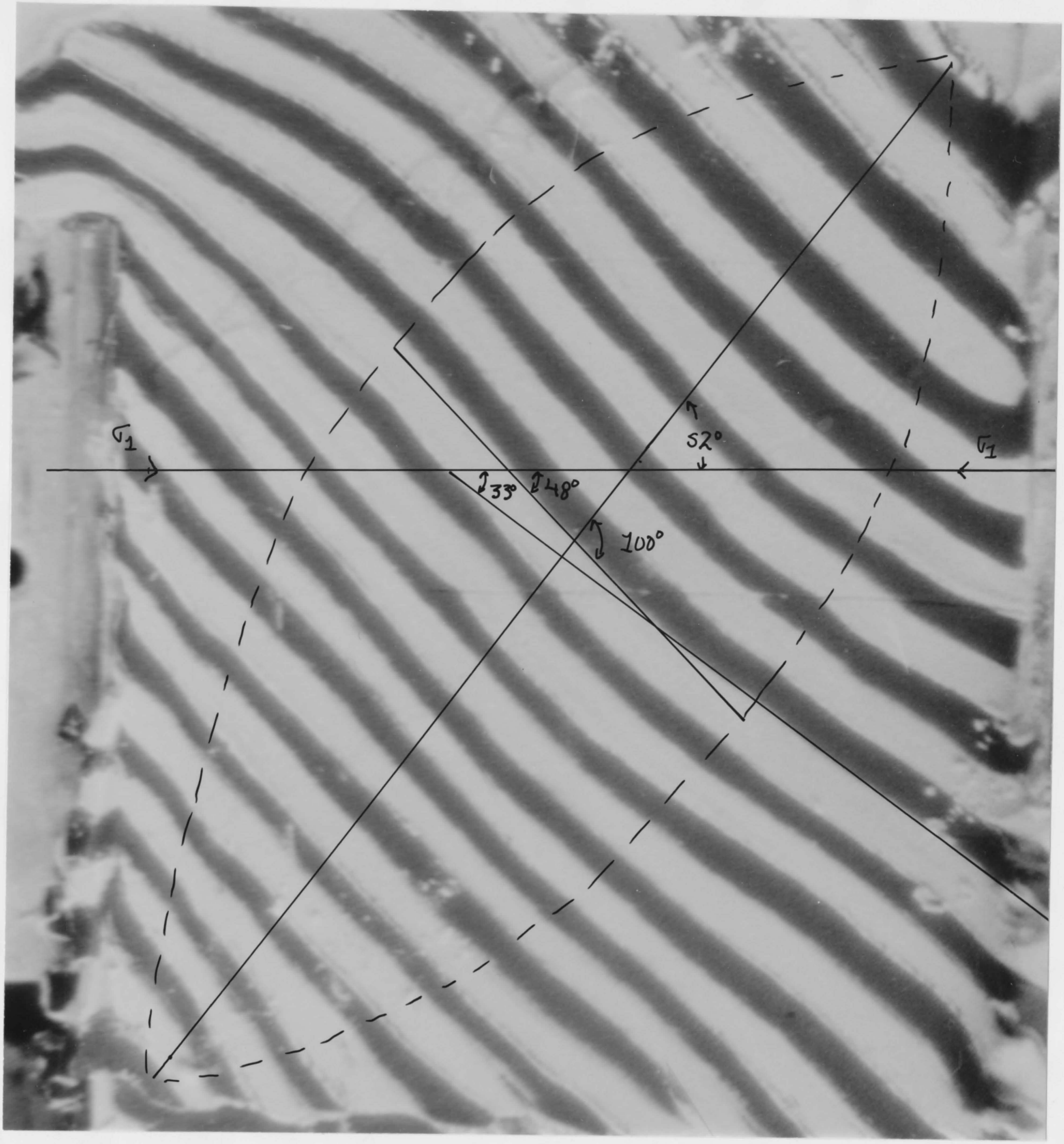

Figure 22. Photograph of Experiment #10 showing measured parameters.

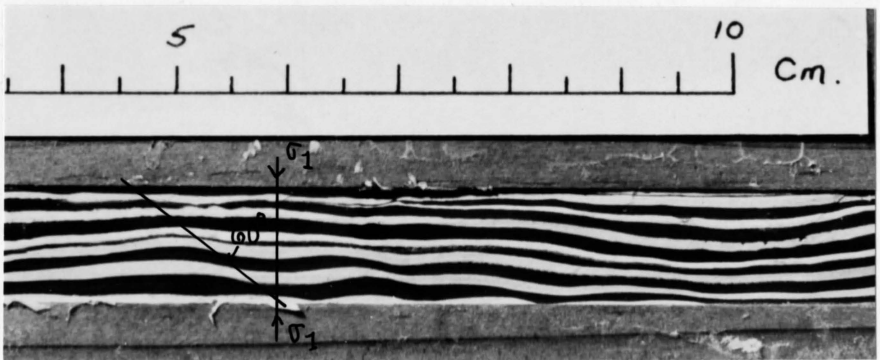

Figure 23. Photograph of Experiment #6 showing measured parameters.

TABLE IV

Conversion table of thickness contours to strain

Figure number	26 & 27	28	29	30	31	32	
Contour line	Strain					Contour line	Strain
1	-.889	-.876	-.853	-.865	-.858	1.0	-.802
2	-.780	-.737	-.703	-.729	-.710	1.5	-.700
3	-.657	-.607	-.559	-.597	-.567	2.0	-.602
4	-.542	-.477	-.411	-.464	-.422	2.5	-.505
5	-.427	-.349	-.264	-.330	-.279	3.0	-.405
6	-.317	-.216	-.116	-.196	-.136	3.5	-.307
7	-.202	-.085	+.031	-.062	+.080	4.0	-.207
8	-.088	+.045	+.179	+.072	+.152	4.5	-.109
9	+.026	+.176	+.326	+.206	+.294	5.0	-.068
10	+.139	+.307	+.473	+.340	+.439	5.5	+.088

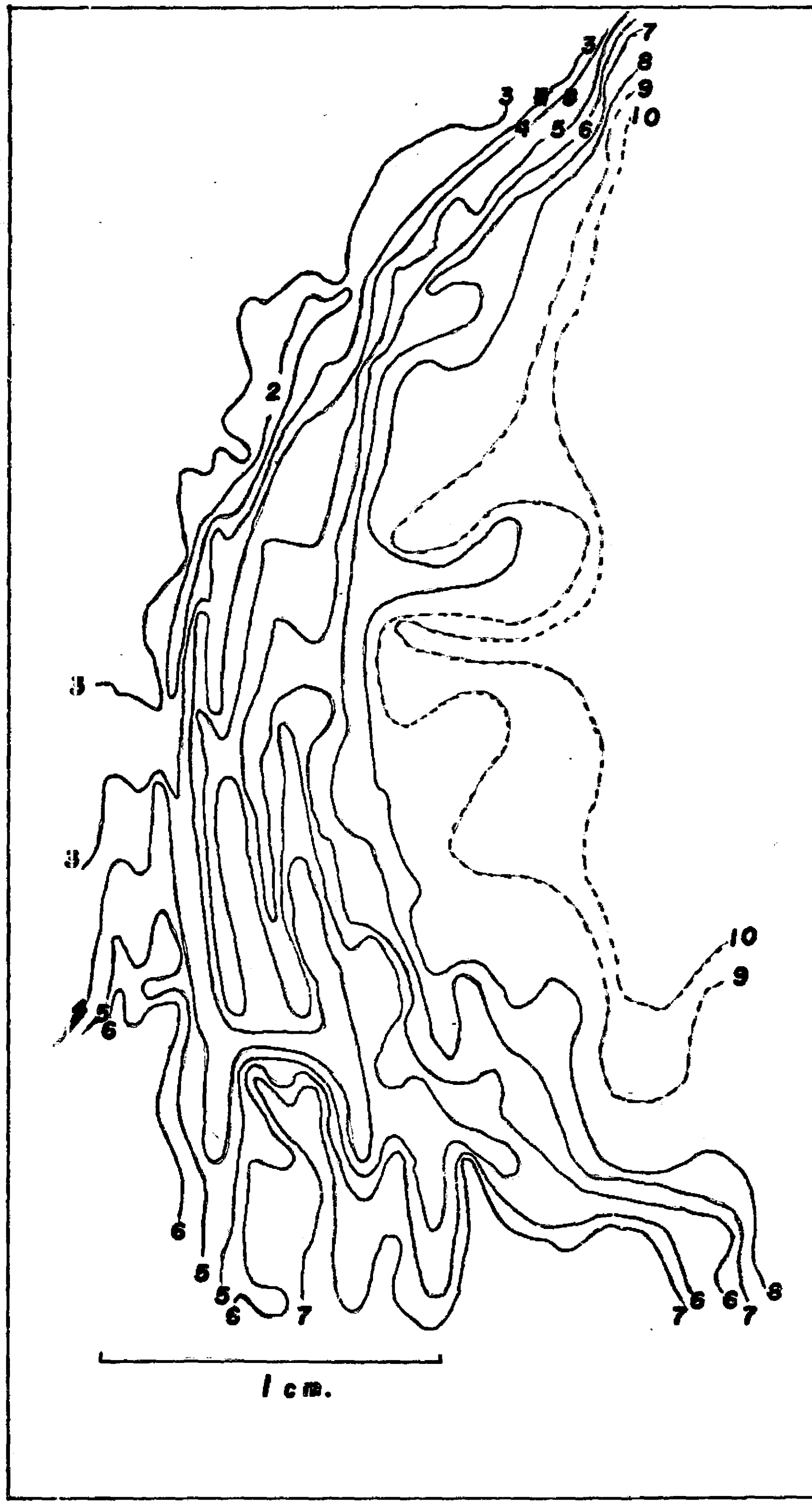

Figure 24. Thickness contours for section 2 of experiment #4.

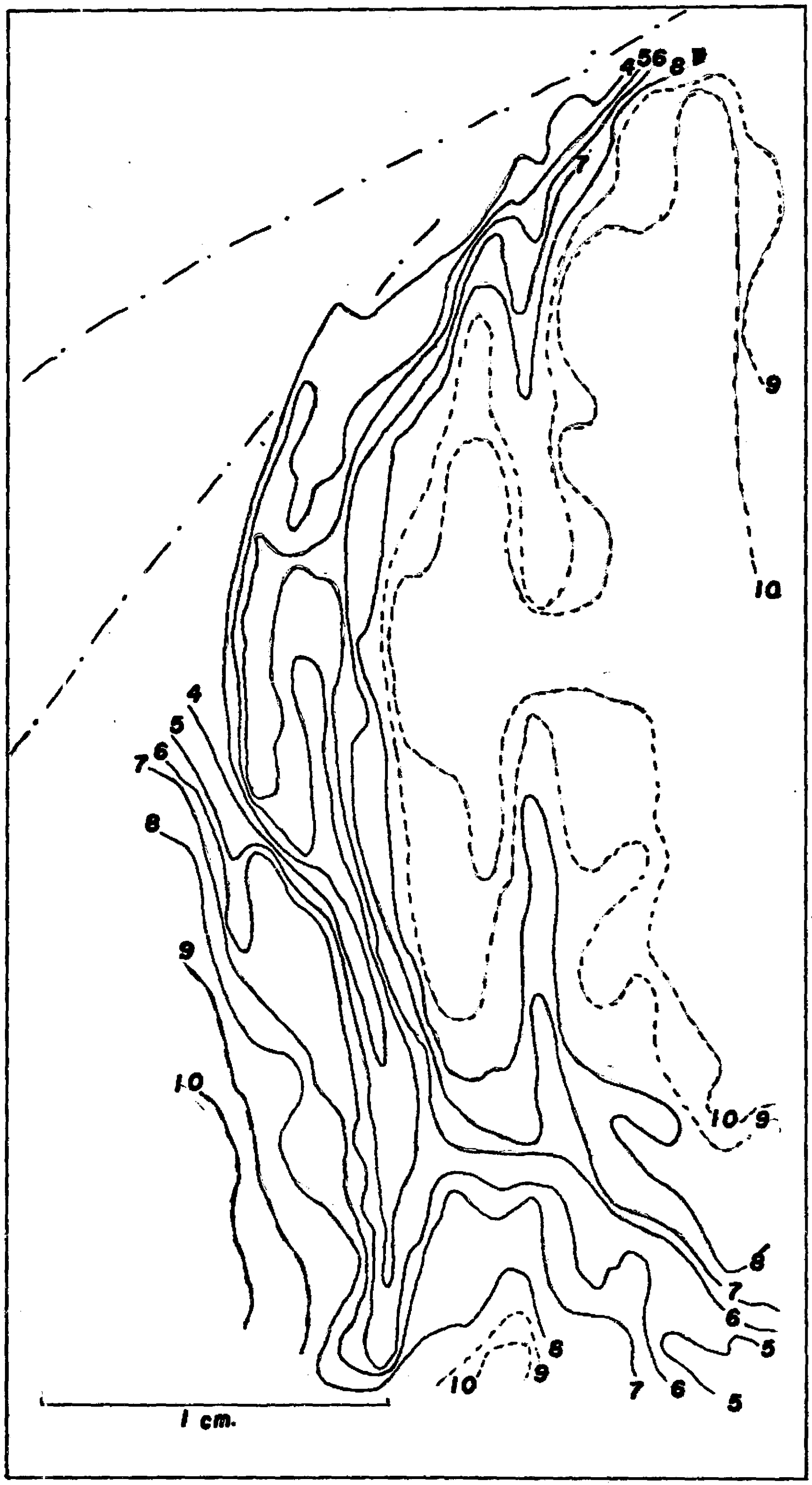

Figure 23. Thickness contours for section 3 of experiment #4.

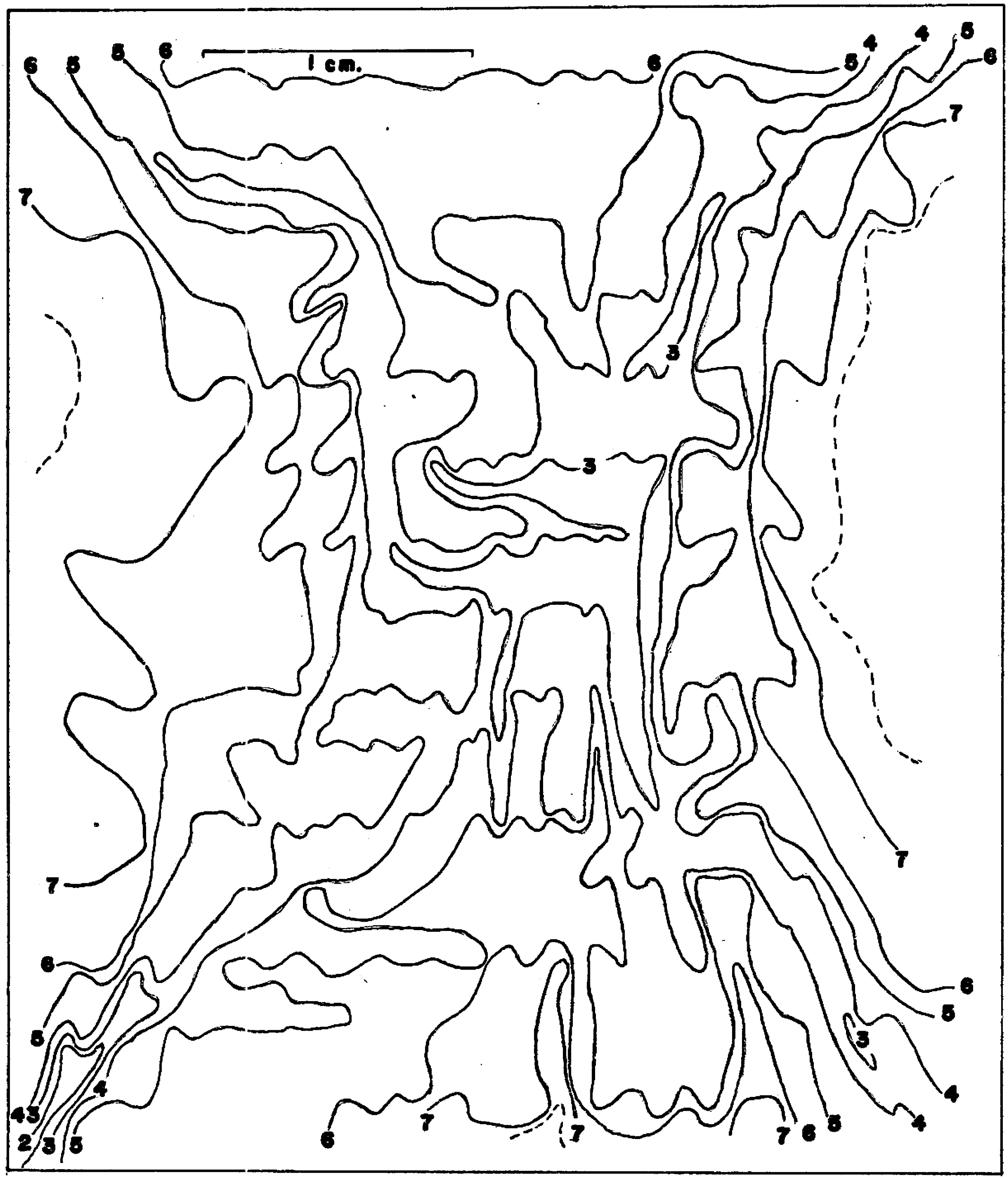

Figure 26. Thickness contours for section 1 of experiment #5.

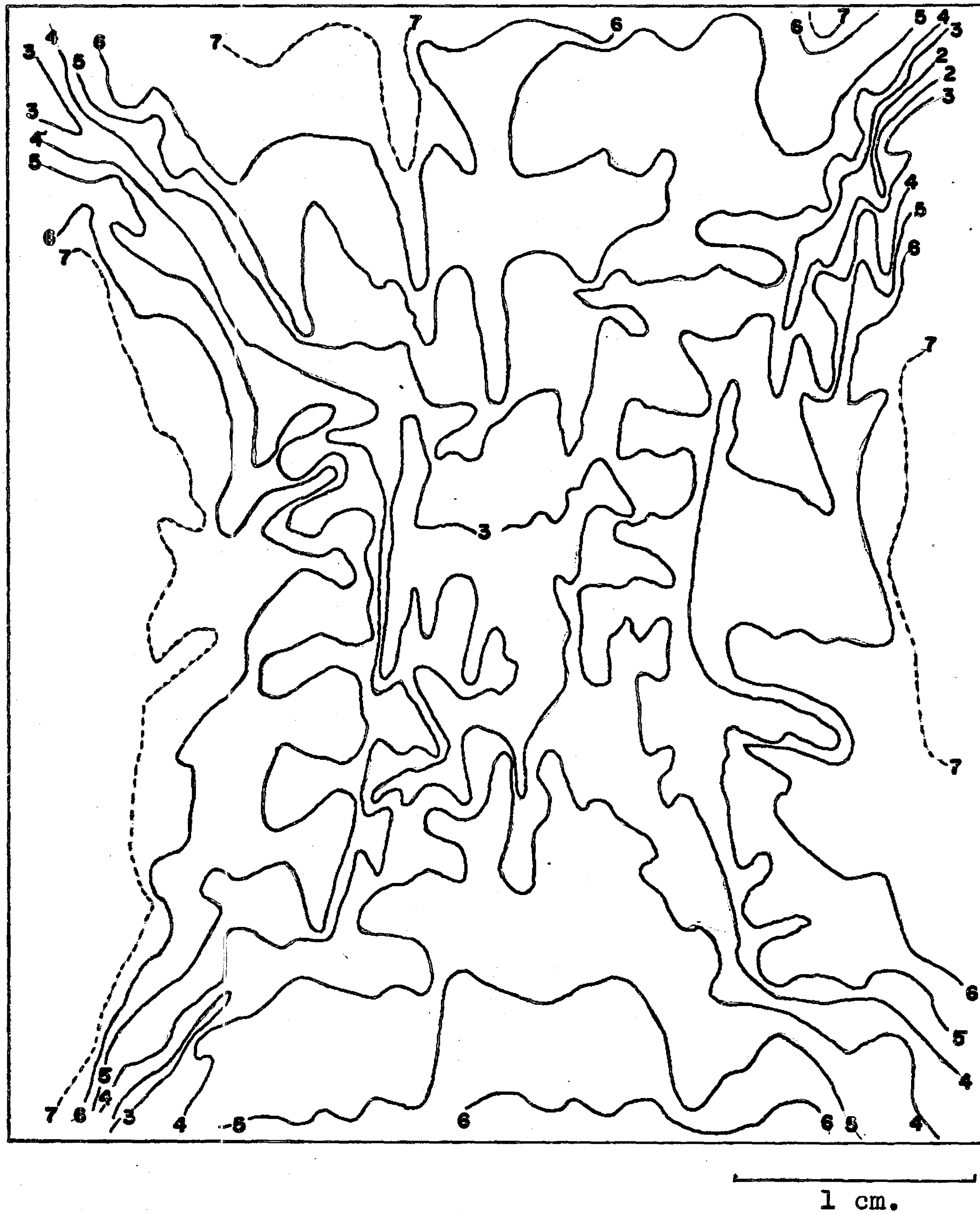

Figure 27. Thickness contours for section 2 of experiment #5.

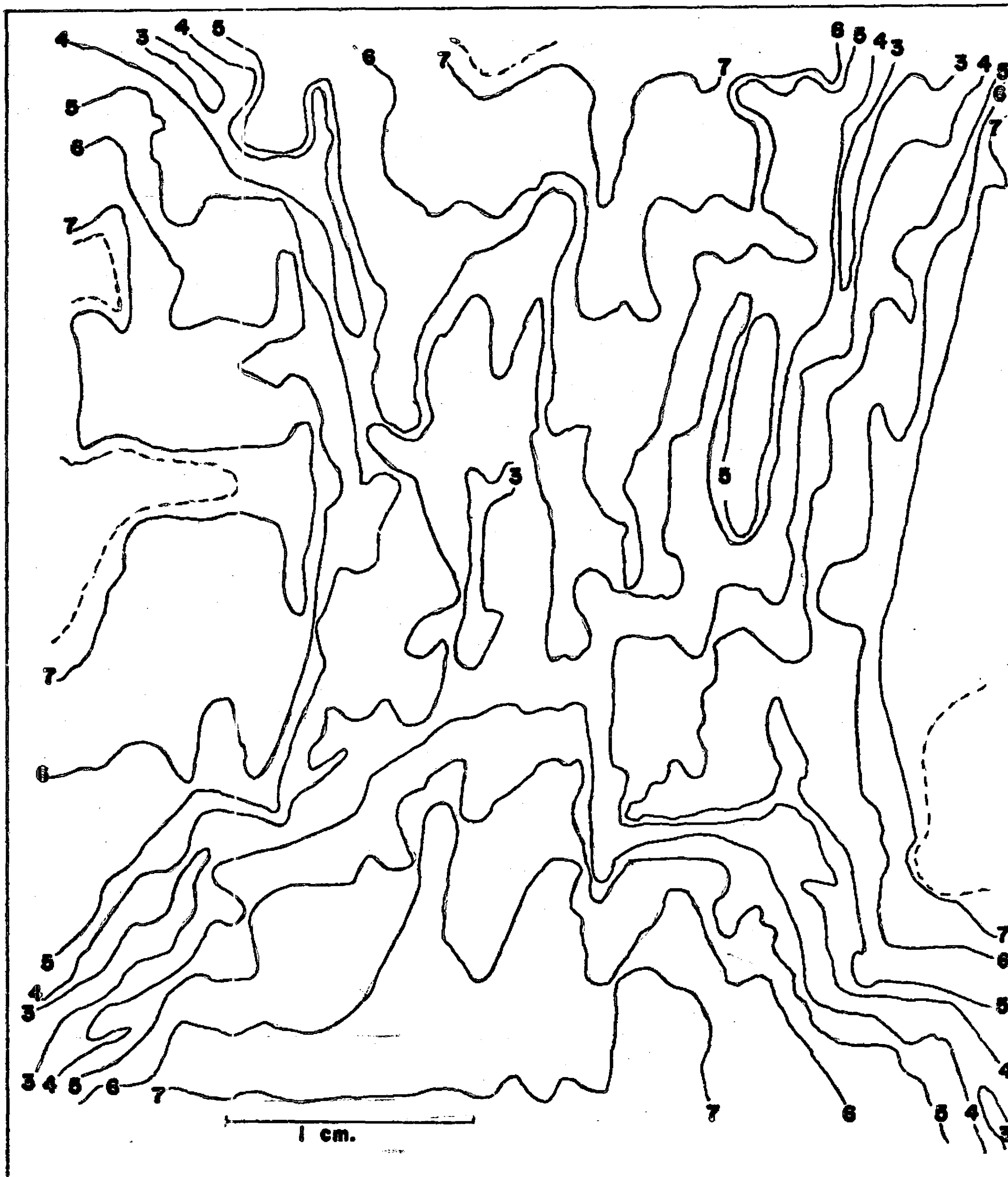

Figure 28. Thickness contours for section 3 of experiment #5.

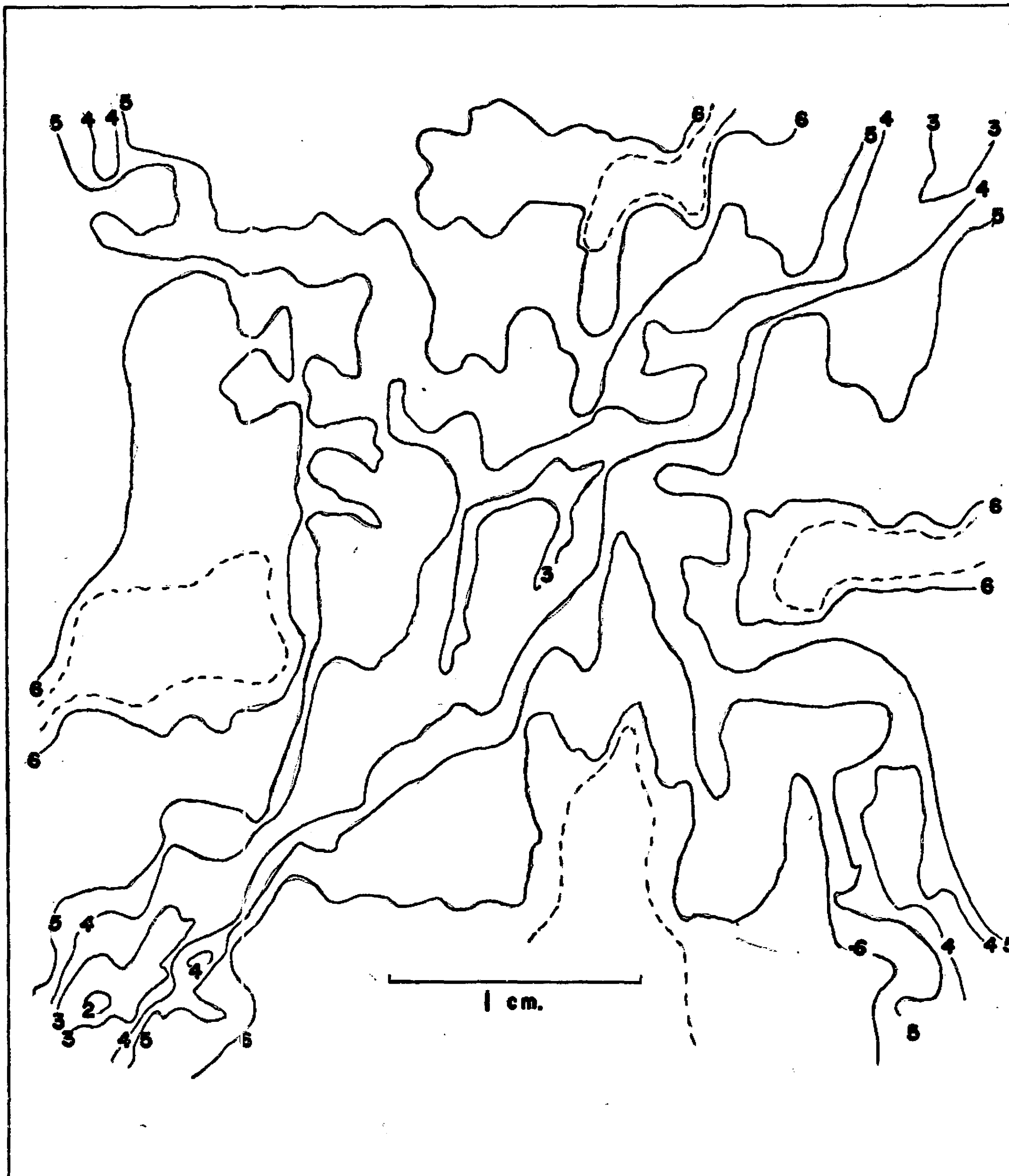

Figure 29. Thickness contours for section 4 of experiment #5.

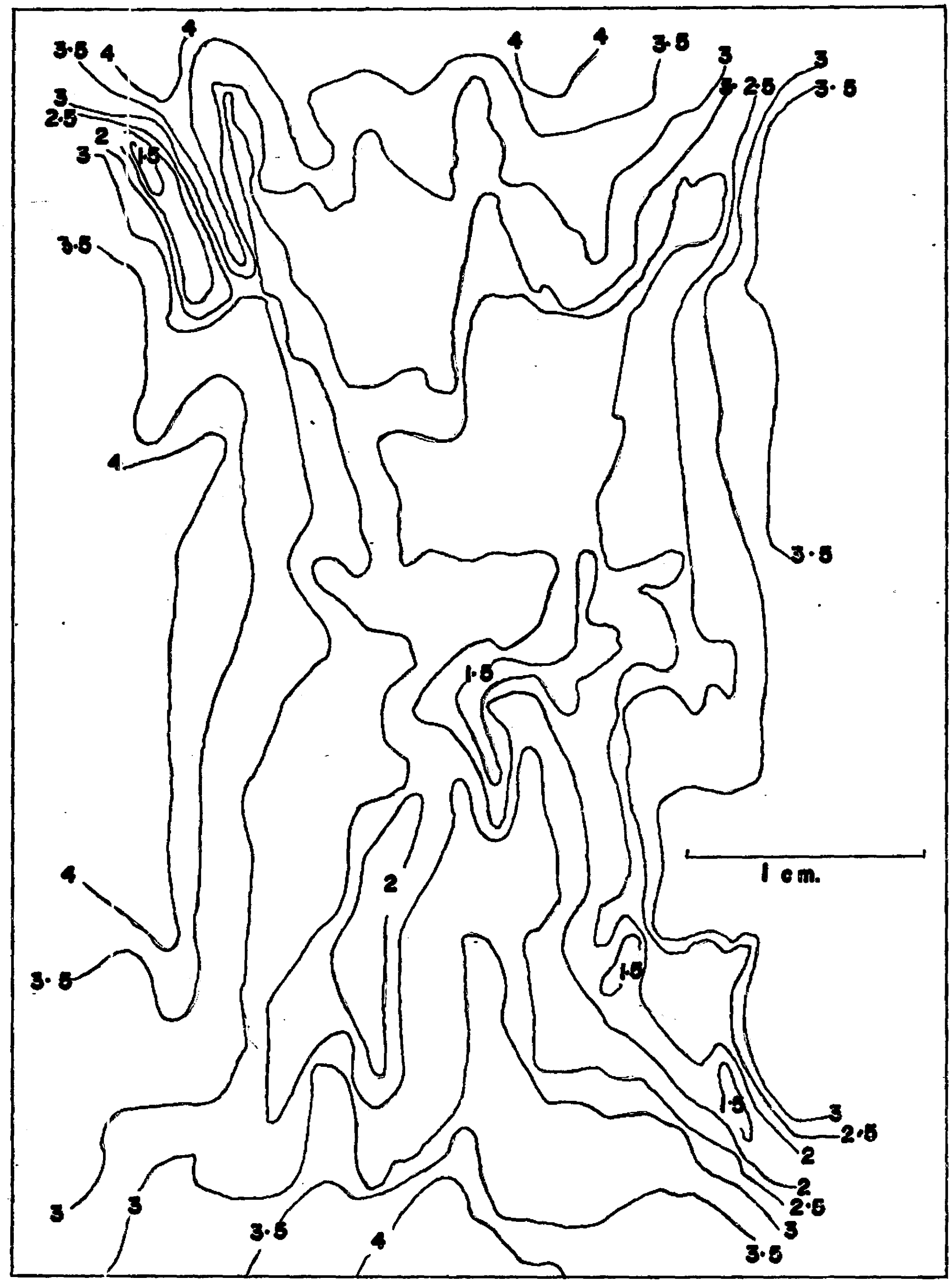

Figure 30. Thickness contours for experiment #7(b).

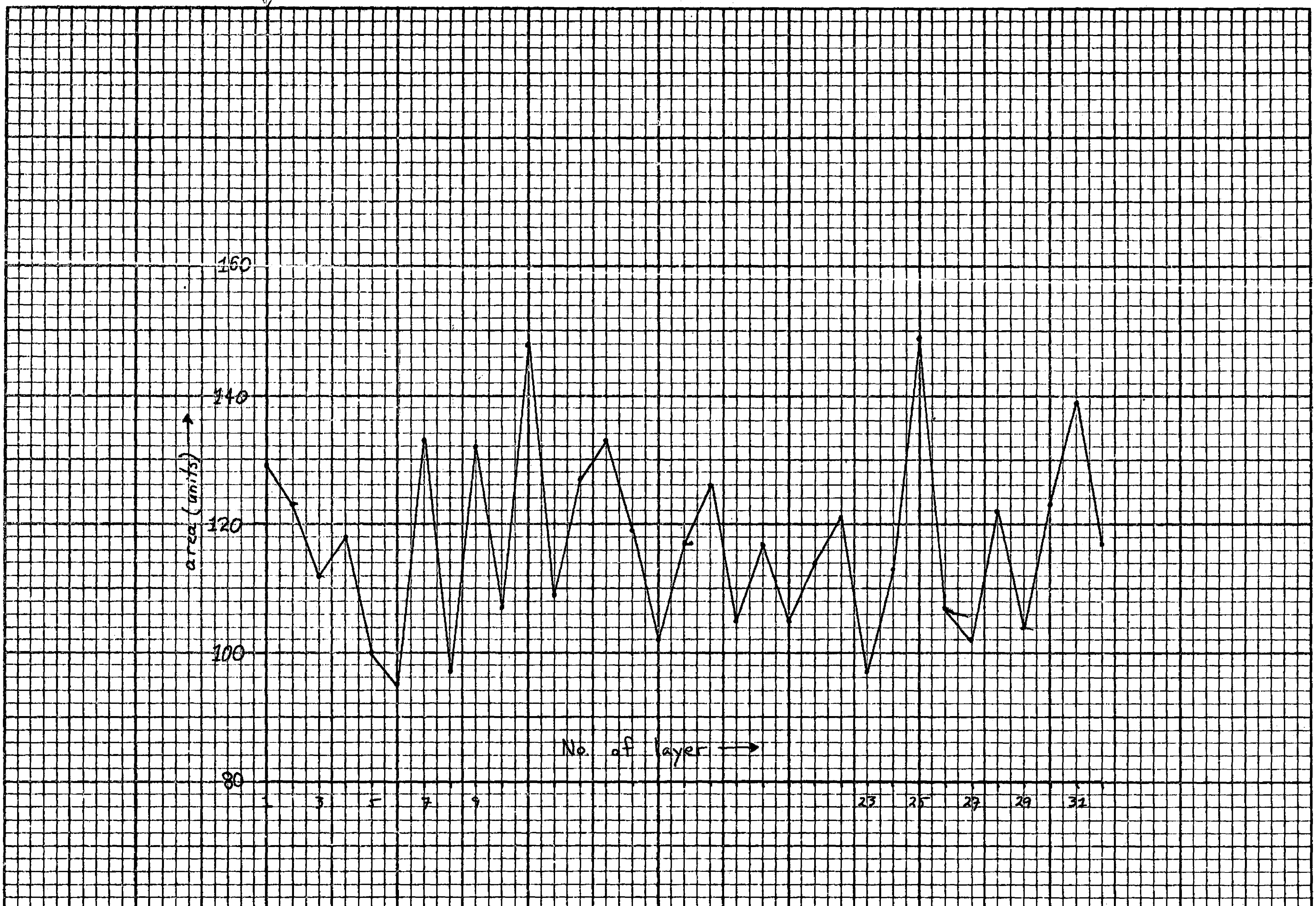

Figure 31. Graph of area vs. no. of layer for face of section 2, Experiment #5. (Area calculated using a planimeter, results are random.)

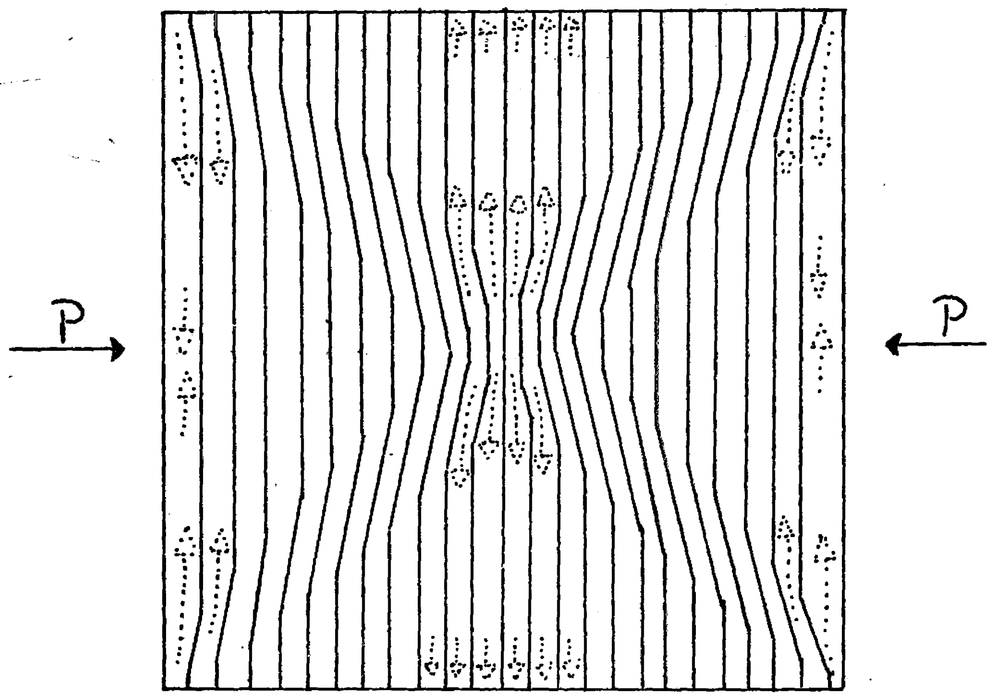

Figure 32. Ductile flow in the multilayer during kink band formation.

(d) Other kink bands produced experimentally

Experiments were run with the layering at various angles to the principal compression direction to observe the structures that resulted and to see how they compared with the experiments run in the orthotropic orientations.

Normal kink bands were developed in experiment #7 (Figures 19 and 20) but one of the conjugate pair was partially suppressed. The principal compression direction (x-direction) didn't bisect the obtuse angle subtended by these conjugate kink bands perhaps suggesting a rotation of σ_1. The kink band orientation change in Figures 19 and 20 is due to homogeneous flattening after the kink bands stopped growing.

The same type of measurements were on these kink bands as on the previous experiments (Table II and Figures 19 and 20). The overall geometry of the kink bands are like the previous ones (experiments #3, #4, #5, and #6).

In experiment #8 no structures developed and this is of particular significance (see section 4(e)).

Experiments #9 and #10 produced single reverse kink bands and their general form was noted. The obtuse angle is very much smaller than for normal kink bands and the width of the kink bands are very much larger.

(e) Isotropic and Anisotropic Orientations

This is an important concept because it explains why some compressed multilayers do not develop instabilities (Experiment #8).

Figure 33 shows how the degree of anisotropy ($\frac{M}{L}$) of a stressed orthotropic material varies in different directions. Cosgrove (1972) suggests that the basic form of the diagram is correct but the actual shape which is determinable by experiment is open to debate. For the materials approximated by figure 35 the isotropic directions are $22\frac{1}{2}^{\circ}$ and $67\frac{1}{2}^{\circ}$ to the x-direction. In zones around these directions the $\frac{M}{L}$ ratio is close to 1. These isotropic zones separate zones of relatively high anisotropy (figure 34). When the principal compression direction is in an isotropic zone the material will show little tendency to develop instabilities. If the principal compression direction falls in an anisotropic zone the material will show little tendency to develop instabilities. If the principal compression direction falls in an anisotropic zone instabilities will develop.

In Experiment #8 the undeformed layering was at 60° to the principal compression direction and in the process of the experiment it rotated to 77°. This rotation of layering during homogenious flattening was also observed by Donath (1968) when he compressed slate to produce reverse kink bands. In experiment #8 the layers probably stayed within the isotropic zones, so instabilities did not develop.

In the field isotropic zones may not be observed. The main reason is that flattening may alter the angle between the axial planes and the layering. It can be seen from the graph in Figure 35 in which the $\frac{M}{L}$ variation is plotted against orientation that flattening may move a material in and out of an isotropic zone. In homogeneous flattening and hence rotation of the layers, material A, in going from a Type I instability to Type II, and vice versa, must pass through a zone of isotropy. It does mot matter what the original orientation was. Material B, with lower anisotropy, stays nearer the isotropic zones and has less chance of instabilities developing.

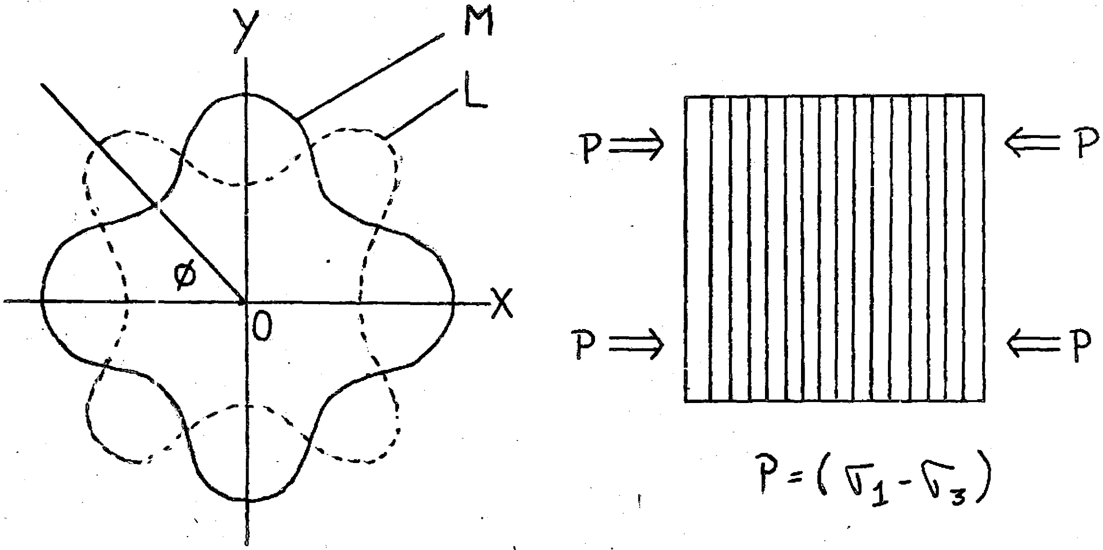

a.) b.)

Figure 35. Model for variations in moduli M and L with orientation to principal axes.

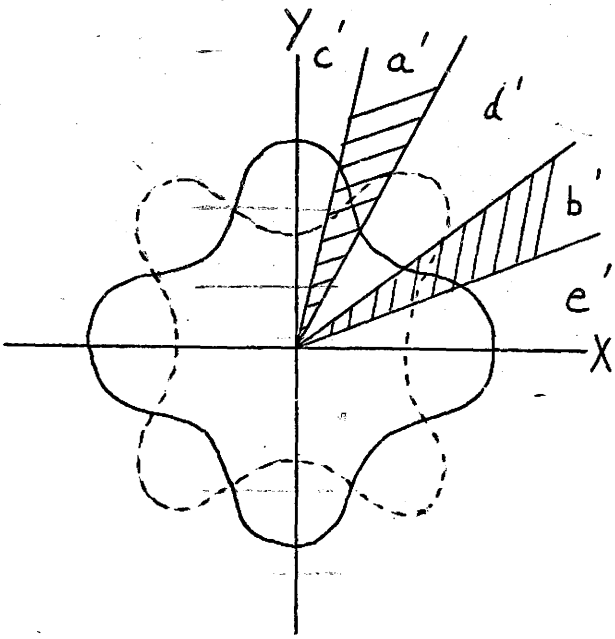

Figure 36. Isotropic (a',b') and anisotropic (c',d',e') zones for model in figure 35.

(After Cosgrove, 1972)

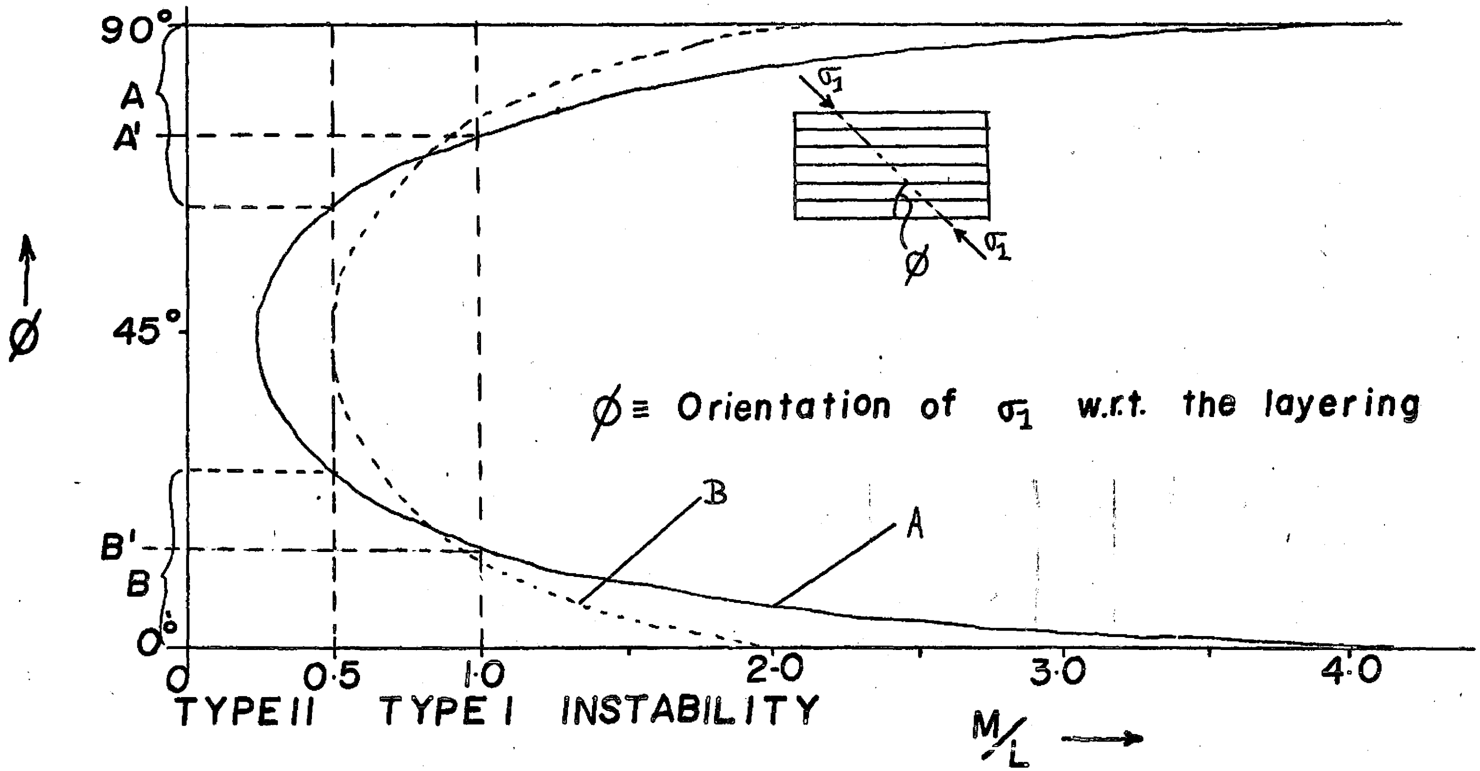

Figure 35. Variation of M/L value with orientation of layering to the principal compression direction.

(After Cosgrove, 1972)

(f) Stress orientation from geometry of normal kink bands

From theory it was shown how instabilities may form normal or at an obtuse angle to the principal compression direction. In certain examples such as symmetric conjugate kink bands the orientation of the stress and strain ellipsoids can be deduced. The σ_1 direction is taken to be parallel to the bisector of the obtuse angle made by the conjugate kink bands and the form gives the σ_2 and σ_3 directions.

There are, however, many structures where the orientation of the principal stressess cannot be obtained immediately from the geometry of the structures. If the principal compression direction is not parallel or normal to the layering (or fabric) one of the conjugate sets of kink bands is supressed. This has been demonstrated in experiment #8. It is not possible to determine the exact orientation of without both sets of kink bands. The σ_1 direction can range from an orientation normal to the axial plane of the structure to an orientation of 45° (Figure 36).

One other effect must be accounted for when determining principal stress directions and that is homogeneous flattening after the final structure has developed. Cosgrove (1972) suggests that the basic symmetry of symmetric Type I and Type II instabilities and asymmetric Type I instabilities is not altered by continued action of σ_1 (homogeneous flattening). However, asymmetric Type II instabilities are altered. This can be seen in experiment #8 where the β angle changed by continual compression after the kink bands stopped growing.

The orientation of the principal **compressive** stress is assumed to be parallel to the bisector of the obtuse angle. In asymmetric Type II instability this direction varies with the amount of flattening.

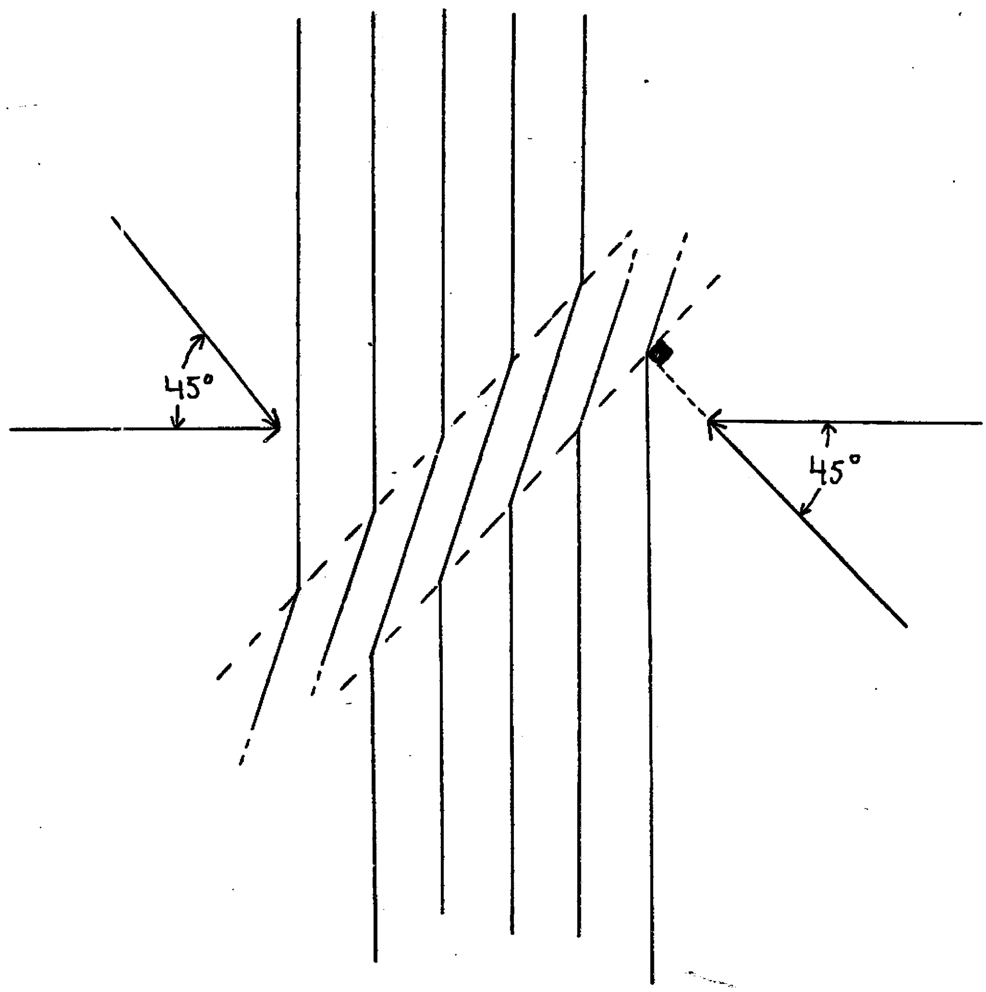

Figure 36. Variation of principal compression direction with a single set of kink bands.

5. Conclusion

Normal kink bands are excellent stress direction indicators but they are not recognized in the field and as a result not used. They could be quite common in deep basin sediments or eugeosynclines where gravity loads are large enough to cause their formation and in isoclinal folds. These features, if found, would give good indications of stress orientation. Cosgrove (private communication) has found these small scale features in both individually folded gneiss belts and relatively undeformed basin sediments. He came to the conclusion that mud cracks, flame structures, etc. may act as a perturbation where the initiation of normal kink bands in eugeosynclinal deposits may develop. Since these deposits are of a great extent laterally σ_2 would equal σ_3 and the orientation of the mud cracks, etc. will govern the orientation of the normal kink bands. The principal compression direction (σ_1) would be normal to the undeformed layers.

More attention should be paid to looking for these features if there is any indication of stress occurring at right angles to the layering or fabric.

6. Appendix

Photographs of the progressive deformation in each experiment performed.

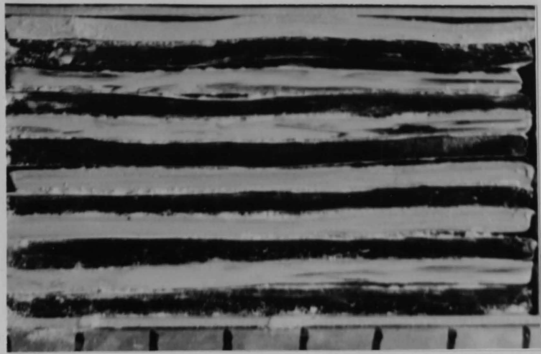

a)

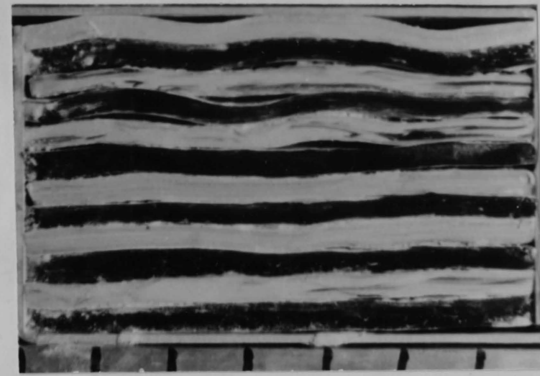

b)

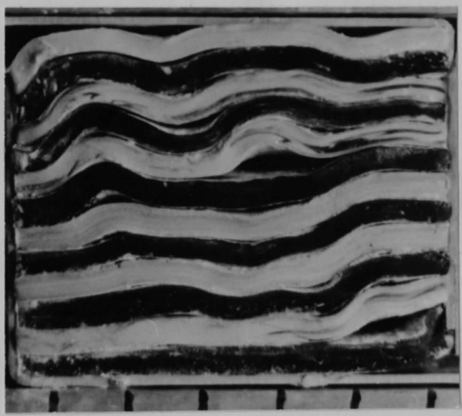

c)

d)

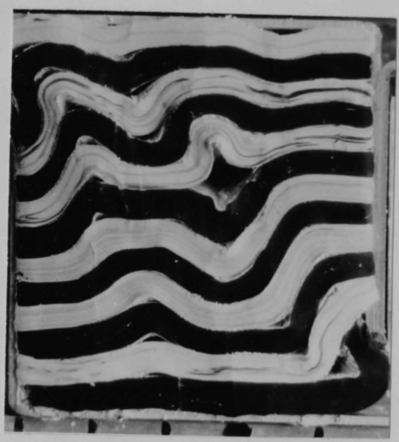

e)

Figure 37. Photographs of Experiment #1.

a) 0% shortening

b) 8% shortening

c) 18% shortening

d) 28% shortening

e) 46% shortening

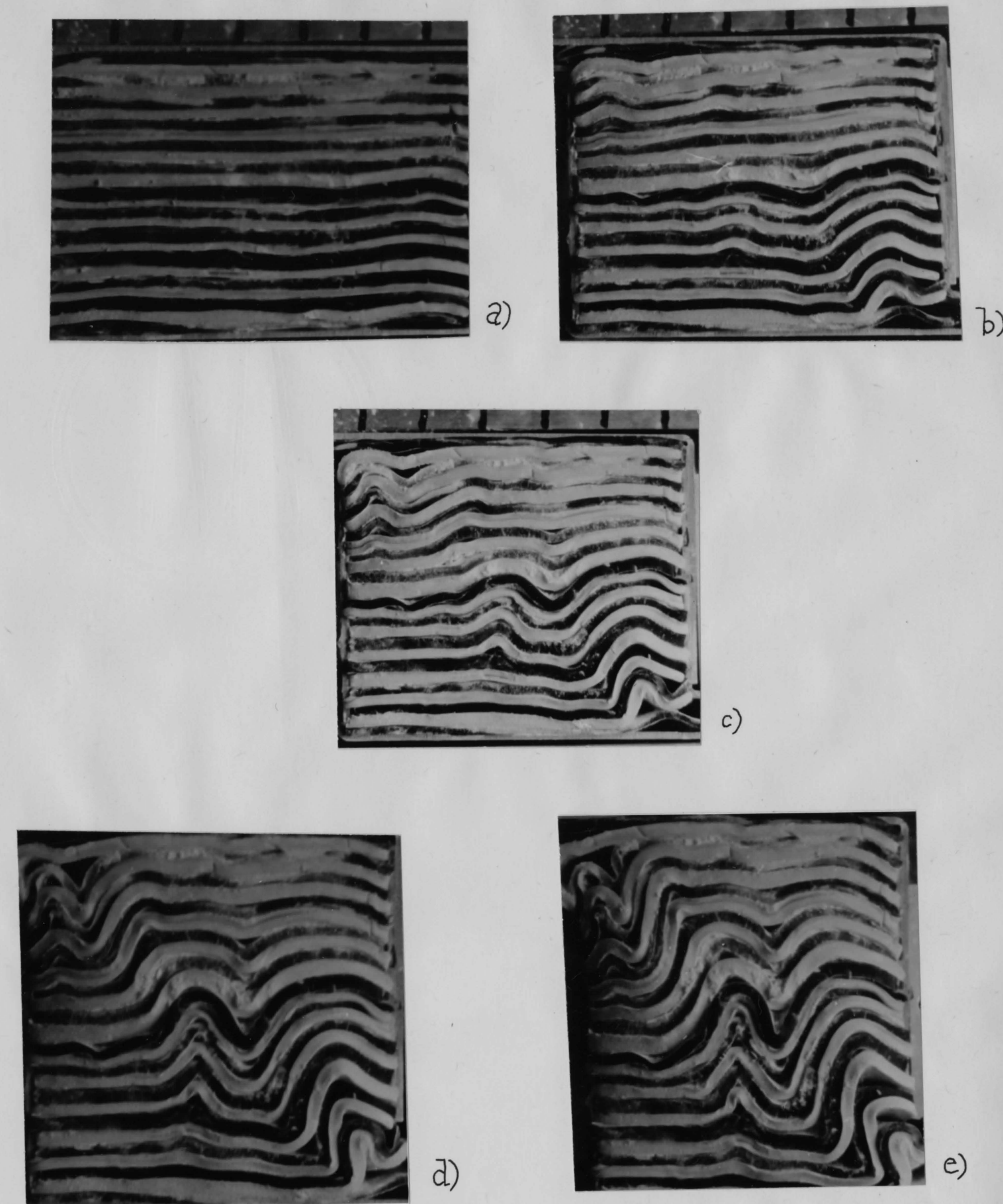

Figure 38. Photographs of Experiment #2.

a) 0% shortening
b) 8% shortening
c) 12% shortening
d) 25% shortening
e) 45% shortening

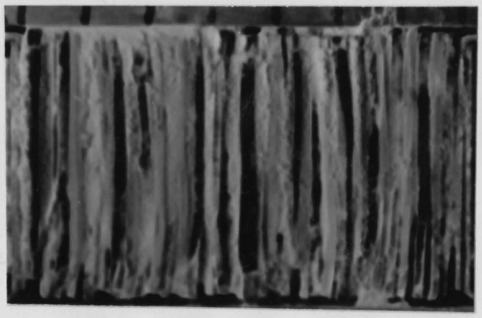
a)

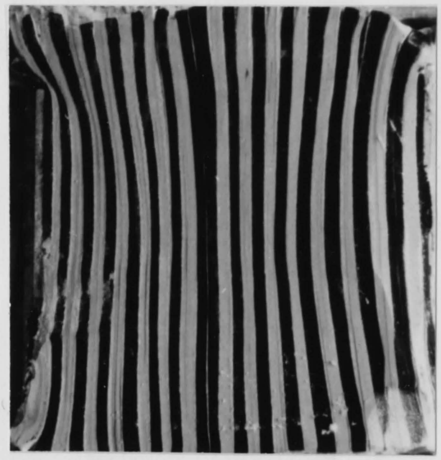
b)


c)

Figure 39. Photographs of Experiment #3

a) 0% shortening c) 50% shortening

b) 35% shortening

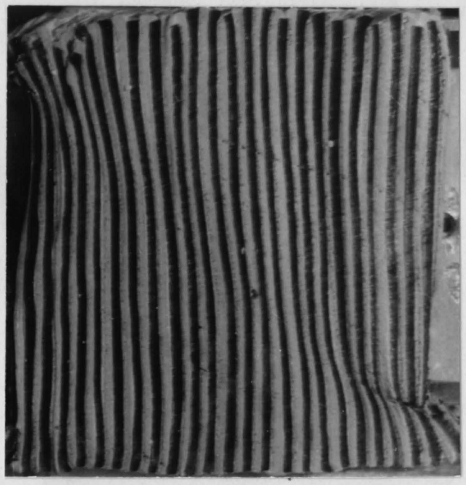

a)

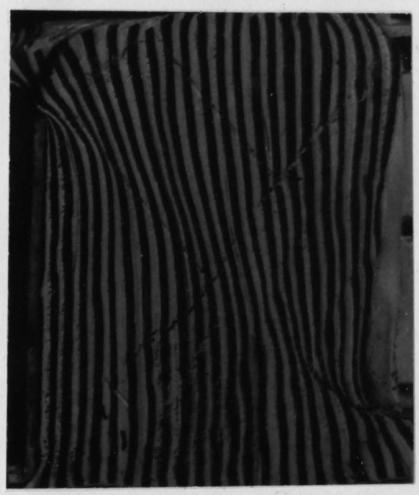

b)

c)

Figure 40........

d)

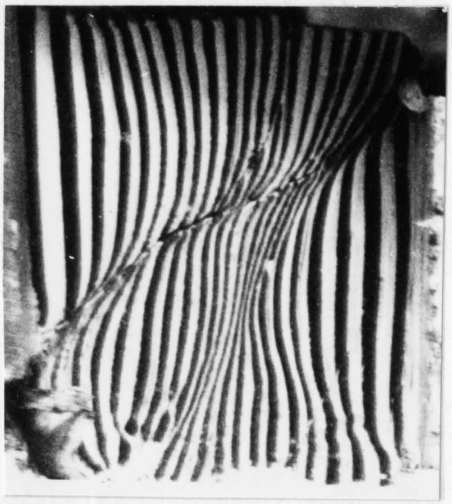

e)

f)

Figure 40. Photographs of Experiment #4

a) 30% shortening c) 55% shortening e) section 3

b) 40% shortening d) section 2 f) section 4

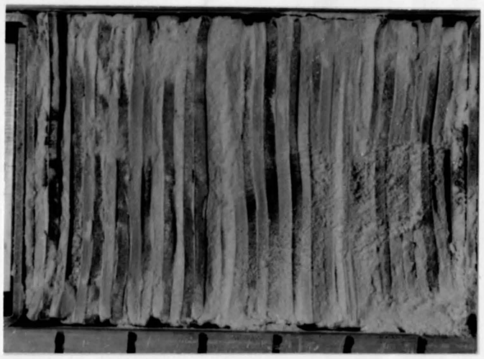

a)

b)

Figure 41 ....

c)

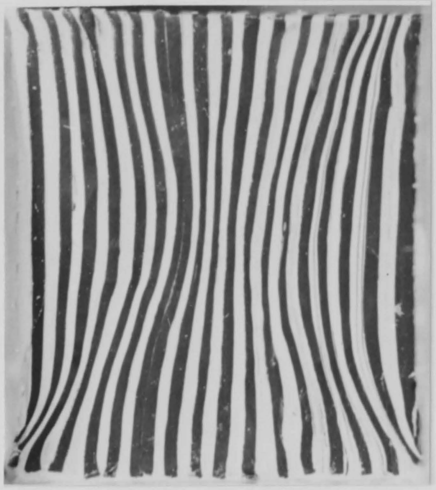

d)

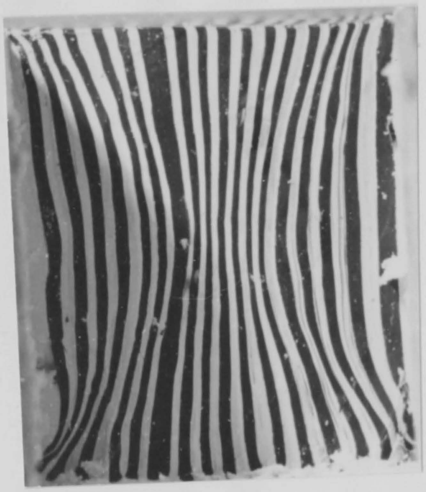

e)

f)

Figure 41. Photographs of Experiment #5.

a) 0% shortening
b) 55% shortening
c) section 2
d) section 3
e) section 4
f) section 5

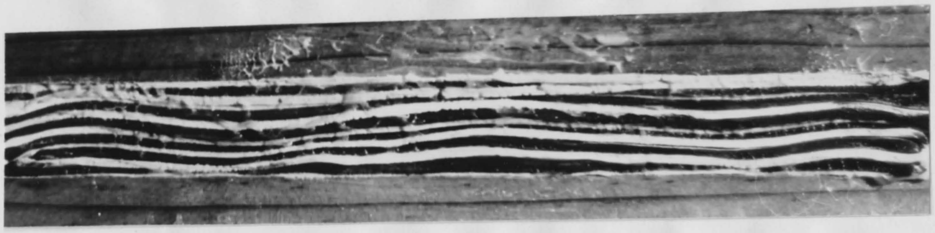

a)

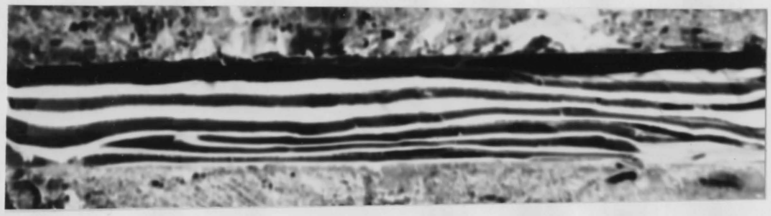

b)

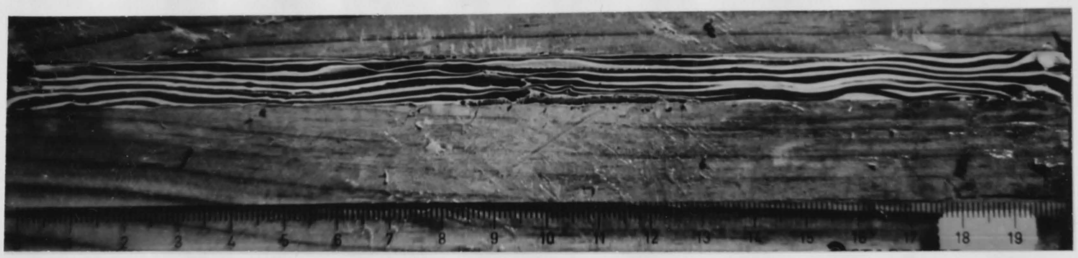

c)

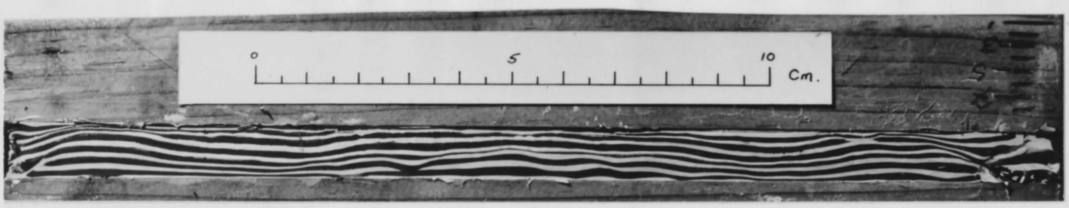

d)

Figure 42. Photographs for Experiment #6.

a) 25% shortening

b) 50% shortening (one end)

c) 50% shrotening (side)

d) 50% shortening (side)

a)

b)

c)

Figure 43. Photographs of Experiment #7.

a) 0% shortening c) 55% shortening

b) 50% shortening

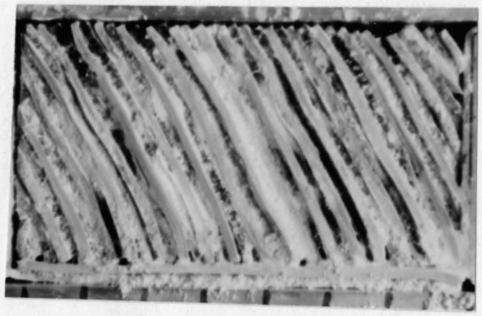

a)

b)

c)

Figure 44. Photographs of Experiment #8.

a) 0% shortening e) 60% shortening

b) 42% shortening

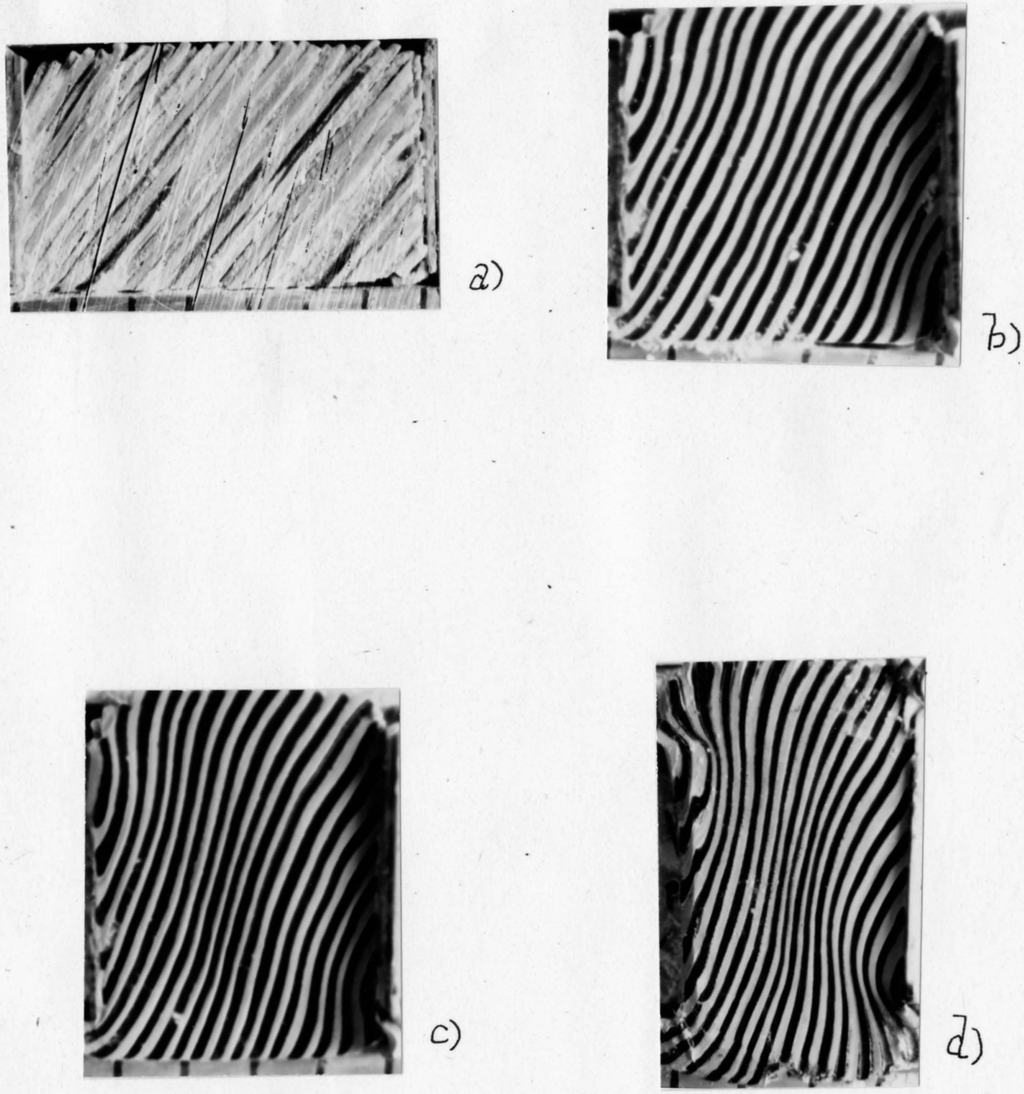

Figure 45. Photographs of Experiment #9.

a) 0% shortening c) 36% shortening

b) 30% shortening d) 53% shortening

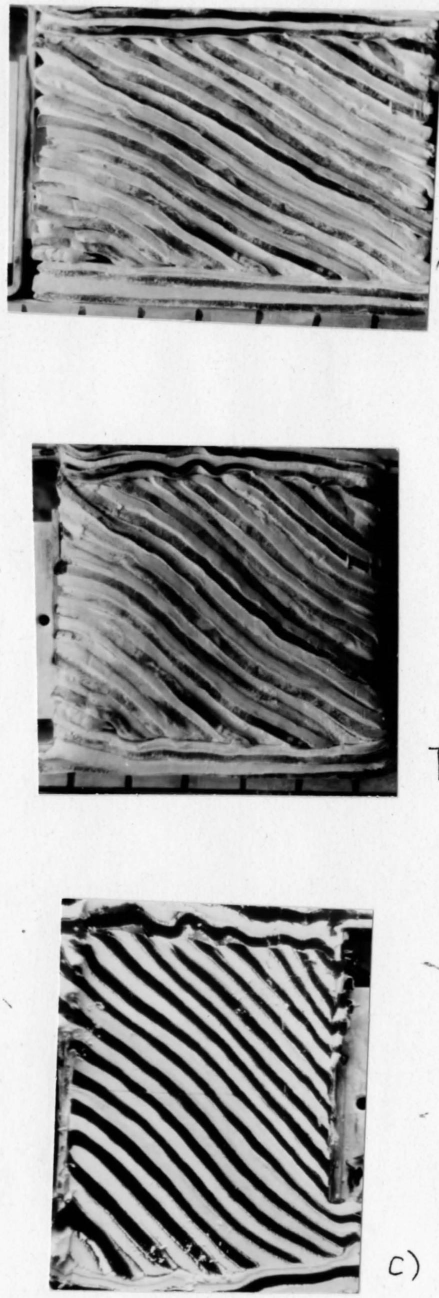

a)

b)

c)

Figure 46. Photographs of Experiment #10.

a) 0% shortening c) 36% shortening

b) 14% shortening

Bibliography

Biot M.A., 1965. Mechanics of Incremental Deformations. Wiley, New York, N.Y., 505pp.

Cobbold P.R., Cosgrove J.W., and Summers J.M., 1971. Development of Internal Structures in Deformed Anisotropic Rocks. Tectonophys 12 , 23-53.

Cosgrove J.W., 1972. Ph.d. Thesis

Donath F.A., 1969. Kink Bands in Brittle Anisotropic Rock. in "Igneous and Metamorphic Geology" Larson L.H., Prinz M., and Manson V. eds., G.S.A. Memoir 115.

Ramsay J.G., 1967. Folding and Fracturing of Rocks. McGraw-Hill, New York, N.Y., 568pp.